Statistical description of complex nuclear phases in supernovae and proto-neutron stars

Ad. R. Raduta[1] and F. Gulminelli[2]

[1] *NIPNE, Bucharest-Magurele, POB-MG6, Romania,*

[2] *LPC (IN2P3-CNRS/Ensicaen et Université), F-14076 Caen cédex, France*

We develop a phenomenological statistical model for dilute star matter at finite temperature, in which free nucleons are treated within a mean-field approximation and nuclei are considered to form a loosely interacting cluster gas. Its domain of applicability, that is baryonic densities ranging from about $\rho > 10^8$ g · cm^{-3} to normal nuclear density, temperatures between 1 and 20 MeV and proton fractions between 0.5 and 0, makes it suitable for the description of baryonic matter produced in supernovae explosions and proto-neutron stars. The first finding is that, contrary to the common belief, the crust-core transition is not first order, and for all subsaturation densities matter can be viewed as a continuous fluid mixture between free nucleons and massive nuclei. As a consequence, the equations of state and the associated observables do not present any discontinuity over the whole thermodynamic range. We further investigate the nuclear matter composition over a wide range of densities and temperatures. At high density and temperature our model accounts for a much larger mass fraction bound in medium nuclei with respect to traditional approaches as Lattimer-Swesty, with sizeable consequences on the thermodynamic quantities. The equations of state agree well with the presently used EOS only at low temperatures and in the homogeneous matter phase, while important differences are present in the crust-core transition region. The correlation among the composition of baryonic matter and neutrino opacity is finally discussed, and we show that the two problems can be effectively decoupled.

PACS numbers: 21.65.Mn, 24.10.Pa, 26.50.+x, 26.60.-c

I. INTRODUCTION

Nuclear matter is not only a theoretical idealization providing benchmark studies of the effective nuclear interaction, but it is also believed to constitute the major baryonic component of massive objects in the universe, as exploding supernovae cores and neutron stars. The structure and properties of these astrophysical objects at baryonic densities exceeding normal nuclear matter density is still highly speculative [1–8]. Conversely for subsaturation densities it is well established that matter is mainly composed of neutrons, protons, electrons, positrons and photons in thermal and typically also chemical equilibrium [9, 10]. Depending on the thermodynamic condition, neutrinos and anti-neutrinos can also participate to the equilibrium.

Such composite matter is subject to the contrasting couplings of the electromagnetic and the strong interaction. Because of the electron screening, the two couplings act on comparable length scales giving rise to the phenomenon of frustration [11–14], well-known in condensed matter physics [15]. Because of this, a specific phase diagram, different from the one of nuclear matter and including inhomogeneous components, is expected in stellar matter [16].

Many theoretical studies exist at zero temperature. In a cold neutron star, going from the dilute crust to the dense core, a transition is known to occur from a solid phase constituted of finite nuclei on a Wigner lattice immersed in a background of delocalized electrons and neutrons, through intermediate inhomogeneous phases composed of non-spherical nuclei (pasta phases), to a liquid phase composed of uniform neutrons, protons and electrons [17–22].

At finite temperature the matter structure and properties are not as well settled. The most popular phenomenological approaches are the Lattimer-Swesty [23] (LS) and the Shen [24] equation of state, recently updated in Ref. [25]. In these standard treatments currently used in most supernovae codes, the dilute stellar matter at finite temperature is described in the baryonic sector as a statistical equilibrium between protons, neutrons, alphas and a single heavy nucleus. The transition to homogeneous matter in the neutron star core is supposed to be first order in these modelizations and obtained through a Maxwell construction in the total density at fixed proton fraction.

It is clear that such single nucleus approximation (SNA) is highly schematic and improvements are possible. Concerning integrated quantities as thermodynamic functions and equations of state, such variables may be largely insensitive to the detailed matter composition [26], though we show in this paper that this is not always the case. However it is also known that the composition at relatively high density close to saturation, together with the pressure and symmetry energy, governs the electron capture rate, which in turn determines the proton fraction at bounce and the size of the homologous core, a key quantity to fix the strength of the shock-wave and the output of the supernovae

explosion [27–32]. Moreover the composition may also affect the nucleosynthesis of heavy elements, which is still poorly understood [33–36], as well as the neutrino scattering through the core after bounce [37, 38], and the cooling rate of neutron stars [39, 40]. For these reasons, in the recent years, many efforts have been done to improve over the simplistic representation of stellar matter given by the SNA approach.

The different modelizations which consider a possible distribution of all different nuclear species inside dilute stellar matter are known under the generic name of Nuclear Statistical Equilibrium (NSE) [41–44]. The basic idea behind these models is the Fisher conjecture that strong interactions in dilute matter may be entirely exhausted by clusterization [45]. In these approaches stellar matter in the baryonic sector is then viewed as a non-interacting ideal gas of all possible nuclear species in thermal equilibrium. The result is that thermodynamic quantities like entropies and pressure appear very similar to the ones calculated with standard approaches, while noticeable differences are seen in the matter composition. In particular an important contribution of light and intermediate mass fragments is seen at high temperature, which is neglected in standard SNA approaches.

The strongest limitation of NSE-based approaches is that they completely neglect in-medium effects, which are known to be very important in nuclear matter. Since the only nuclear interactions are given by the cluster self-energies, the homogeneous matter composing the neutron star core cannot be modelized, nor it can be the phenomenon of neutron drip in the inner crust, well described by mean-field models [46]. As a consequence, these models cannot be applied at densities close to saturation and the crust-core transition cannot be described.

To overcome this problem, different microscopic [47–50] as well as phenomenological [51] approaches have been developed in the very recent past. In this paper we would like to introduce a phenomenological model that treats the nuclei component within an improved NSE, while it describes the unbound protons and neutrons in the finite temperature Hartree-Fock approximation.

The plan of the paper is as follows. The first part of the paper is devoted to the description of the model. The clusterized component, the homogeneous component, the properties of the mixture and the lepton sector are described in successive sections together with their thermodynamic properties. A particular attention is devoted to the modelization of the crust-core transition. We show that the inclusion of excluded volume is sufficient to describe the transition from the clusterized crust to the homogeneous core, and that this transition is continuous. Different generic as well as specific arguments are given against the possibility of a first-order transition. The second part of the paper gives some results relevant for the star matter phenomenology. The first section shows observables following constant chemical potential paths, in order to connect the observables with the properties of the phase diagram. Then the behavior of the different quantities for constant proton fractions is displayed in order to compare with more standard treatments of supernova matter. Finally the last section addresses the problem of neutrino trapping and the interplay between the matter opacity to neutrinos and matter composition. Conclusions and outlooks conclude the paper.

II. THE MODEL

The model aims to describe the thermal and chemical properties of nuclear matter present in supernovae and (proto)-neutron stars at densities ranging from the normal nuclear density ρ_0 to $\approx 10^{-6}\rho_0$, temperatures between 0 and 20 MeV and proton concentration between 0.5 and 0. In this regime, the star matter typically consists of a mixture of nucleons, light and heavy nuclear clusters, neutrinos (if we consider the thermodynamic stage where neutrinos are trapped), photons and a charge neutralizing background of electrons and positrons.

As there is no interaction among electrons, neutrinos, photons and nuclear matter, the different systems may be treated separately and their contributions to the global thermodynamic potential and equations of state added-up.

In the grancanonical ensemble this reads,

$$G(\beta, \beta\mu_n, \beta\mu_p, \beta\mu_e, V) = G^{(bar)}(\beta, \beta\mu_n, \beta\mu_p, V) + G^{(lep)}(\beta, \beta\mu_e, V) + G^{(\gamma)}(\beta, V), \tag{1}$$

where the grancanonical potential,

$$\begin{aligned} G(\beta, \beta\mu_n, \beta\mu_p, \beta\mu_e, V) &= \ln \mathcal{Z}_{gc}(\beta, \beta\mu_n, \beta\mu_p, \beta\mu_e, V) \\ &= \bar{S}\left[\beta, -\beta\mu_n, -\beta\mu_p\right], \end{aligned} \tag{2}$$

is the Legendre transformation of the entropy S with respect to the fixed intensive variables. In the previous equations V is an arbitrary macroscopic volume and $\mathcal{Z}_{gc}$ is the grancanonical partition sum.

The observables conjugated to the ones fixed by the reservoir and geometry can be immediately calculated as partial derivatives of G. Thus, the total energy density is

$$
\begin{aligned}
e &= -\frac{1}{V}\left(\frac{\partial G}{\partial \beta}\right)|_{\beta\mu_n,\beta\mu_p,V} \\
&= e^{(bar)} + e^{(lep)} + e^{(\gamma)},
\end{aligned}
\tag{3}
$$

the different particle densities are

$$
\rho_i = \frac{1}{V}\left(\frac{\partial G}{\partial(\beta\mu_i)}\right)|_{\beta,\beta\mu_j,V},
\tag{4}
$$

where $i = n, p, e$, and finally the total pressure is

$$
p = \frac{G}{\beta V} = p^{(bar)} + p^{(lep)} + p^{(\gamma)}.
\tag{5}
$$

A. The baryon sector

The light and heavy nuclei are assumed to form a gas of loosely-interacting clusters which coexist in the Wigner-Seitz cell with a homogeneous background of delocalized nucleons. To avoid exceeding the normal nuclear density and naturally allow for homogeneous-unhomogeneous matter transition, nuclei and nucleons are forbidden to occupy the same volume. In the following we start describing the modelization of these two components separately, and we turn successively to the properties of the mixture obtained when the two are supposed to be simultaneously present in the Wigner-Seitz cell.

1. The homogeneous nuclear matter component

Mean-field models constitute a natural choice for approaching interacting particle systems. By introducing a mean-field potential, the physical problem is reduced to the simplified version of a system of non-interacting particles. Effective nucleon-nucleon interactions allow one to express the system average energy as a simple single-particle density functional, and to cast the nuclear matter statistics in a way which is formally very similar to an ideal Fermi gas[52].

The mean field energy density of an infinite homogeneous system $e^{(HM)} = <\hat{H}>_0 /V$ is a functional of the particle densities ρ_q and kinetic densities τ_q for neutrons ($q = n$) or protons ($q = p$). At finite temperature, the mean field approximation consists in expressing the grancanonical partition function of the interacting particle system as the sum of the grancanonical partition function of the corresponding independent-particle system associated to the mean-field single-particle energies, with the temperature weighted difference between the average single-particle energy ($<\hat{W}>_0 = -\partial_\beta \ln \mathcal{Z}_0$) and the mean-field energy

$$
\ln \mathcal{Z}^{(HM)} \approx \ln \mathcal{Z}_0^{(HM)} + \beta\left(\left\langle\hat{W}\right\rangle_0 - \left\langle\hat{H}\right\rangle_0\right).
\tag{6}
$$

The one body partition sum is defined as:

$$
\mathcal{Z}_0^{(HM)} = Tr[e^{-\beta(\hat{W}_0 - \mu_n\hat{N}_n - \mu_p\hat{N}_p)}] = \mathcal{Z}_0^n \mathcal{Z}_0^p,
\tag{7}
$$

and can be expressed as a function of the neutron and proton kinetic energy density :

$$
\frac{\ln \mathcal{Z}_0^q}{V} = 2\int_0^\infty \ln(1 + e^{-\beta(\frac{p^2}{2m_q^*}-\mu_q')})\frac{4\pi p^2}{h^3}dp = \frac{\hbar^2}{3m_q^*}\beta\tau_q,
\tag{8}
$$

with

$$\rho_q = 2 \int_0^\infty n_q(p) \frac{4\pi p^2}{h^3} dp, \tag{9}$$

$$\tau_q = 2 \int_0^\infty \frac{p^2}{\hbar^2} n_q(p) \frac{4\pi p^2}{h^3} dp. \tag{10}$$

In these equations the effective chemical potential μ'_q includes the self energies according to $\mu'_q = \mu_q - \partial_{\rho_q} e^{(HM)}$, $m^*_{n,p} = \left(\partial e^{HM} / \partial \tau_{n,p} \right)^{-1}/2$ are the neutron (proton) effective mass, and the factor 2 comes from the spin degeneracy.

Equation (9) establishes a self-consistent relation between the density of q-particles ρ_q and their chemical potential μ_q. Introducing the single particles energies $\epsilon^i_q = \frac{p_i^2}{2m_q^*} + \partial_{\rho_q} e^{(HM)}$, the above densities can be written as regular Fermi integrals by shifting the chemical potential according to $\mu'_q = \mu_q - \partial_{\rho_q} e^{HM}$. The Fermi-Dirac distribution indeed reads:

$$n_q(p) = \frac{1}{1 + \exp(\beta(p^2/2m_q^* - \mu'_q))}. \tag{11}$$

Eqs. (11) and (9) define a self-consistent problem since m_q^* depends on the densities. For each couple (μ'_n, μ'_p) a unique solution (ρ_n, ρ_p) is found by iteratively solving the self-consistency between $\rho_{n,p}$ and $m^*_{n,p}$. Then Eq. (10) is used to calculate $\tau_{n,p}$.

At the thermodynamic limit the system volume V diverges together with the particle numbers $\langle \hat{N}_n \rangle$, $\langle \hat{N}_p \rangle$, and the thermodynamics is completely defined as a function of the two particle densities (ρ_n, ρ_p), or equivalently the two chemical potentials (μ_n, μ_p).

With Skyrme based interactions, the energy density of homogeneous, spin saturated matter with no Coulomb effects is written as:

$$
\begin{aligned}
e^{(HM)} = \ & \frac{\hbar^2}{2m}(\tau_n + \tau_p) \\
+ \ & t_0(x_0 + 2)(\rho_n + \rho_p)^2/4 - t_0(2x_0 + 1)(\rho_n^2 + \rho_p^2)/4 \\
+ \ & t_3(x_3 + 2)(\rho_n + \rho_p)^{\sigma+2}/24 - t_3(2x_3 + 1)(\rho_n + \rho_p)^\sigma(\rho_n^2 + \rho_p^2)/24 \\
+ \ & (t_1(x_1 + 2) + t_2(x_2 + 2))(\rho_n + \rho_p)(\tau_n + \tau_p)/8 + (t_2(2x_2 + 1) - t_1(2x_1 + 1))(\rho_n\tau_n + \rho_p\tau_p)/8, \tag{12}
\end{aligned}
$$

where $t_0, t_1, t_2, t_3, x_0, x_1, x_2, x_3, \sigma$ are Skyrme parameters.

Several Skyrme potentials have been developed over the years for describing the properties of both infinite nuclear matter and atomic nuclei, and address the associated thermodynamics. It was thus in particular shown that nuclear matter manifests liquid-gas like first-order phase transitions up to a critical temperature [53–57].

In order to make direct quantitative comparisons between our model and the one of Lattimer and Swesty [23], through this paper nucleon-nucleon interactions are accounted for according to the SKM* parameterization [58] if not explicitly mentioned otherwise. Table I summarizes the force parameters while the main properties of nuclear matter are summarized in Table II.

The thermodynamic properties of the system are best studied introducing the constrained entropy:

$$s_c^{(HM)} = s^{(HM)} - \beta e^{HM}, \tag{13}$$

where the entropy density is nothing but the Legendre transform of the mean field partition sum:

$$s^{(HM)} = \ln \mathcal{Z}^{(HM)}/V + \beta \left(e^{(HM)} - \mu_n \rho_n - \mu_p \rho_p \right). \tag{14}$$

Instabilities are then recognized as local convexities of the constrained entropy at a given temperature $T = 1/\beta$ in the two-dimensional density plane (ρ_n, ρ_p). In the presence of an instability, the system entropy can be maximized by phase mixing, which corresponds to a linear interpolation in the density plane. This geometrical construction corresponds to the well-known Gibbs equality between all intensive parameters of two coexisting phases in equilibrium:

TABLE I: SKM* force parameters [58].

Parameter	Value
t_0 (MeV fm^3)	-2645
t_1 (MeV fm^5)	410
t_2 (MeV fm^5)	-135
t_3 (MeV fm$^{3+3\sigma}$)	15595
x_0	0.09
x_1	0.
x_2	0.
x_3	0.
σ	1/6

TABLE II: Infinite nuclear matter and surface properties of SKM* force [58].

Observable	Value
E/A (MeV)	-15.78
K_∞ (MeV)	216.7
m^*/m	0.79
C_{sym} (MeV)	30.03
ρ_0 (fm^{-3})	0.1603
a_s (MeV)	17.51
k_s	3.74

$$
\begin{aligned}
\beta^{(1)} &= \beta^{(2)}; \\
\mu_q^{(1)} &= \mu_q^{(2)}, \quad q = n, p; \\
P^{(1)} &= P^{(2)}.
\end{aligned}
\tag{15}
$$

Phase diagrams of SKM* nuclear matter are illustrated in Figs. 1, 2 and 3 for three values of temperature $T =$ 1.6, 5 and, respectively, 10 MeV in $\mu_n - \mu_p$ (left panels) and $\rho_n - \rho_p$ (right panels) representations. As it is customary in nuclear matter calculations, the system is charge neutral in the sense that the electromagnetic interaction has been artificially switched off. In the star matter case the proton electric charge has to be taken into account, and compensated by the electron charge to give a net zero charge. The resulting Coulomb interaction energy will be discussed in the next chapter. Full lines correspond to the phase coexistence region and dashed lines mark the borders of the instability region, the so-called spinodal surface.

As one may notice, a large portion of the density and chemical potential plane is characterized by the instability even at temperatures as high as 10 MeV. Inside the phase coexistence in the density representation, the mean field solution is unphysical at thermal equilibrium if matter is uniquely composed of homogeneously distributed (uncharged) protons and neutrons. In the case of stellar matter, the entropy convexity properties have to be examined only after considering all the different constituents, which can very drastically change the properties of the phase diagram. As we will show in the next sections, the introduction of electrons has the effect of making the Gibbs construction unphysical, while the introduction of clusterized matter has the effect of stabilizing the unstable mean field solution.

2. The clusterized nuclear matter component

As we have discussed in the previous section, in a wide region of temperature and density, uncharged uniform nuclear matter is unstable with respect to density fluctuations. If such fluctuations occur on a macroscopic scale, a first-order liquid-gas phase transition follows. Inside the spinodal surface however, finite wavelength fluctuations may also occur, leading to spontaneous cluster formation. Spinodal decomposition and nucleation are indeed known to
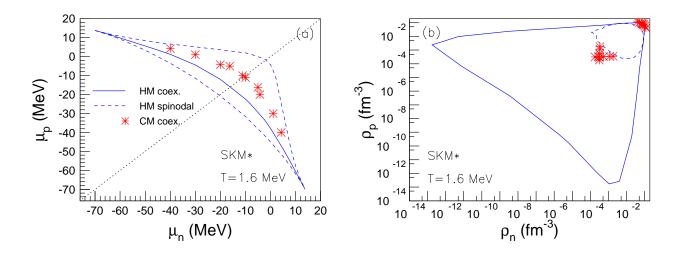
FIG. 1: (Color online) $\mu_p - \mu_n$ (left) and $\rho_p - \rho_n$ (right) representations of the phase diagrams of the charge-neutral homogeneous infinite nuclear matter described by the SKM* interaction (lines) and net-charge neutralized clusterized nuclear matter (stars) corresponding to T=1.6 MeV. In the case of the uniform system, the dashed lines mark the borders of the spinodal zone, while the solid line marks the coexistence region. These results are independent of the chosen confining volume $V = 2.9 \cdot 10^4$ fm^3 except in the low density region of the phase diagram of the clusterized matter system in $\rho_p - \rho_n$ coordinates, which is affected by finite size effects (see text).
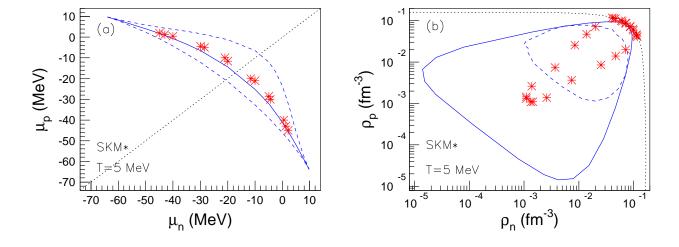

FIG. 2: (Color online) The same as in Fig. 1 for T=5 MeV. For symbol and line codes, see Fig. 1.

constitute the dynamical mechanisms leading to phase separation in macroscopic uncharged systems. As we will show in the following, in the presence of the repulsive long range Coulomb interaction among protons, which is screened by the leptons only on macroscopic scales, phase separation is quenched in stellar matter and the instability is cured by the formation of nuclear clusters, that is clusters in the femtometer scale.

One possibility to account for the thermal and phase properties of a clusterized matter sub-system is to use a statistical model with cluster degrees of freedom. Several such models have been so far proposed for the study of condensation close to the critical point [45], nuclear multifragmentation [59–62] and compact stars [42–44]. They basically consist in the estimation of the number of microscopic states compatible with the thermodynamic macroscopic constraints.

Considering that the center of mass of the clusters can be treated as classical degrees of freedom, the grancanonical
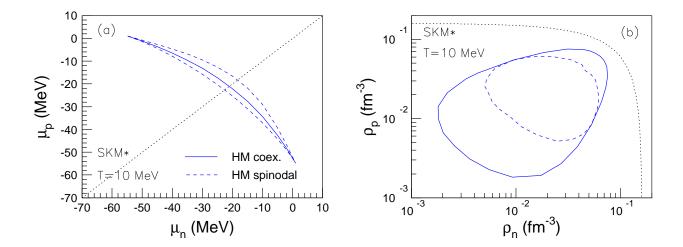
FIG. 3: (Color online) The same as in Fig. 1 for $T=10$ MeV.

partition function of the clustered system reads:

$$
\begin{aligned}
\mathcal{Z}^{(cl)}_{\beta,\beta\mu_n,\beta\mu_p} &= \sum_C W_C = \sum_C \frac{1}{N_C!} \int \frac{d^3r_1...d^3r_{N_C}d^3p_1...d^3p_{N_C}}{h^{3N_C}} \exp\left[-\beta\left(E_C - \mu_n N_C - \mu_p Z_C\right)\right] \\
&= \sum_C \frac{1}{N_C!} \exp\left(-\beta E_{int}(C)\right) \cdot \\
&\quad \cdot \prod_{i=1}^{N_C}\left[V_i^{free}(C)\left(\frac{mA_iT}{2\pi\hbar^2}\right)^{3/2}\rho(A_i,Z_i,\epsilon_i)\exp\left(\beta B_i - \beta\epsilon_i + \beta\mu_n N_i + \beta\mu_p Z_i\right)\right].
\end{aligned}
\tag{16}
$$

Here C denotes a generic cluster configuration $C = \{(A_1,Z_1,\epsilon_1),...,(A_{N_C},Z_{N_C},\epsilon_{N_C})\}$ defined by the mass number A_i, the proton number Z_i and the excitation energy ϵ_i of each constituent nuclear state indexed by i, whose binding energy is B_i and level density is $\rho(A_i,Z_i,\epsilon_i)$; $E_{int}(C)$ represents the inter-cluster configuration dependent interaction energy, and $V_i^{free}(C) < V$ is the volume accessible to cluster i which is not excluded by the presence of the other clusters. Because of the short range of the nuclear force, this excluded volume correction can be viewed as a first-order approximation to the nuclear part of the interaction energy in the spirit of the Van der Waals gas. More sophisticated in-medium corrections can in principle be also added as modifications of the cluster self-energies B_i [50]. Because of this, we will consider that the interaction energy only contains the Coulomb electrostatic energy of the configuration.

To obtain the so-called NSE approach, one has to neglect all inter-particle interactions except the cluster self-energies, leading to :

$$
\mathcal{Z}^{(cl)}_{\beta,\beta\mu_n,\beta\mu_p} \approx \mathcal{Z}^{(cl)}_0 = \sum_C \frac{V^{N_C}}{N_C!}\prod_{i=1}^{N_C}\left[\left(\frac{mA_iT}{2\pi\hbar^2}\right)^{3/2}\rho(A_i,Z_i,\epsilon_i)\exp\left(\beta B_i - \beta\epsilon_i + \beta\mu_n N_i + \beta\mu_p Z_i\right)\right].
\tag{17}
$$

The advantage of this simplification is that a completely factorized expression for the partition sum can be obtained, leading to analytical expressions for all thermodynamic quantities. Indeed any configuration (C) can be ordered as

$$
(C) = \{\underbrace{T_1,T_1,\ldots,T_1}_{n_1(C)},\underbrace{T_2,T_2,\ldots,T_2}_{n_2(C)},\ldots\},
\tag{18}
$$

where $n_i(C) = n_{A_i,Z_i,\epsilon_i}(C)$ gives the multiplicity of clusters of type $T_i = \{A_i,Z_i,\epsilon_i\}$. Equation (17) becomes:

$$\mathcal{Z}_0^{(cl)} = \prod_{i=1}^{\infty} \sum_{n_i=0}^{\infty} \frac{1}{n_i!} \left[z_{\beta,\beta\mu_n,\beta\mu_p} \left(A_i, Z_i, \epsilon_i \right) \right]^{n_i}, \tag{19}$$

with

$$z_{\beta,\beta\mu_n,\beta\mu_p} \left(A_i, Z_i, \epsilon_i \right) = \left(\frac{mA_iT}{2\pi\hbar^2} \right)^{3/2} \rho(A_i, Z_i, \epsilon_i) \exp \left(\beta B_i - \beta\epsilon_i + \beta\mu_n N_i + \beta\mu_p Z_i \right). \tag{20}$$

Eq. (19) is not yet an analytically tractable expression, because of the infinite number of possible excited states for each nuclear isotope (A_i, Z_i). The internal degrees of freedom can be however integrated over giving

$$\mathcal{Z}_{\beta,\beta\mu_n,\beta\mu_p}^{(NSE)} = \prod_{A,Z=1}^{\infty} \sum_{n_{A,Z}=0}^{\infty} \frac{1}{n_{A,Z}!} \left[z_{\beta,\beta\mu_n,\beta\mu_p} \left(A, Z \right) \right]^{n_{A,Z}}, \tag{21}$$

where $z_{\beta,\beta\mu_n,\beta\mu_p} \left(A, Z \right)$ is the standard grancanonical partition sum for a single nucleus of mass A and charge Z:

$$\begin{aligned}
z_{\beta,\beta\mu_n,\beta\mu_p} \left(A, Z \right) &= \left(\frac{mAT}{2\pi\hbar^2} \right)^{3/2} \int d\epsilon \rho(A_i, Z_i, \epsilon) \exp \left(\beta B_i - \beta\epsilon + \beta\mu_n N + \beta\mu_p Z \right) \\
&= \left(\frac{mAT}{2\pi\hbar^2} \right)^{3/2} g_\beta(A, Z) \exp \left(\beta B_i + \beta\mu_n N + \beta\mu_p Z \right),
\end{aligned} \tag{22}$$

and $g_\beta(A, Z)$ is a temperature dependent degeneracy.

While elegant and analytically tractable, Eq. (21) represents a correct estimation of Eq. (16) if and only if the interactions are fully exhausted by clusterization.

For this reason, in this work we will consider only Eq. (16), which we will estimate numerically with a precise, efficient and well-tested Metropolis-Monte-Carlo technique [62], and calculate relevant thermodynamic observables other than the ones fixed by the exterior as ensemble averages. For the configuration-defined quantities, $X_C = A_{tot}(C)$, $Z_{tot}(C)$, $E_{tot}(C)$:

$$\begin{aligned}
A_{tot}(C) &= \sum_{i=1}^{N_C} A_i \\
Z_{tot}(C) &= \sum_{i=1}^{N_C} Z_i \\
E_{tot}(C) &= \sum_{i=1}^{N_C} \left(-B_i + \epsilon_i \right),
\end{aligned} \tag{23}$$

the corresponding ensemble averaged density reads:

$$<x> = \frac{1}{V} \frac{\sum_C X_C W_C}{\sum_C W_C}, \tag{24}$$

and stability is systematically checked against an increase of the considered volume V.

For each sampled configuration (C), we evaluate the Coulomb interaction energy in the Wigner-Seitz approximation [17],

$$V_{Coulomb}(C) = \sum_{i=1}^{N_C} \frac{3}{5} c(\rho) \frac{e^2 Z_i^2}{r_0 A_i^{1/3}}, \tag{25}$$

with

$$c(\rho) = 1 - \frac{3}{2}\left(\frac{\rho_e}{\rho_{0p}}\right)^{1/3} + \frac{1}{2}\left(\frac{\rho_e}{\rho_{0p}}\right),\tag{26}$$

accounting for the screening effect of electrons. $\rho_{0p} = Z/A\rho_0$ denotes the proton density inside the nuclei and ρ_e is the electron density. Net charge neutrality of the system imposes the electron density ρ_e to be equal to the proton density ρ_p.

The total pressure results:

$$\begin{aligned}\beta p &= \left(\frac{\partial G^{(cl)}}{\partial V}\right)|_{\beta,\beta\mu_n,\beta\mu_p}\\ &= \frac{N_C}{V} - \frac{3}{5}\frac{\beta}{2V}\left(\frac{1}{n^{1/3}} - \frac{1}{n}\right)\sum_i \frac{e^2 Z_i^2}{r_0 A_i^{1/3}}\\ &= \beta\left(p^{(cl)} + p^{(lattice)}\right).\end{aligned}\tag{27}$$

Here $p^{(cl)}$ originates from clusters translational motion and $p^{(lattice)}$ is the so-called lattice Coulomb pressure.

Concerning the excluded volume, the result of the N_C integrals over the coordinate space corrected for the volume excluded by each cluster, V_i, can be re-casted as a global configuration-dependent factor $\chi(C)V^{N_C}$ as,

$$V(V - V_1)(V - V_1 - V_2)...(V - V_1 - V_2 - ... - V_{N_C-1}) = \chi V^{N_C}.\tag{28}$$

For the clusters we assume the following properties:

- clusters binding energies are described by a liquid-drop parameterization,

$$B(A,Z) = \left(a_v A - a_s\left(1 - Tf(T)\right)A^{2/3}\right)\left(1 - a_I(A - 2Z)^2/A^2\right)\tag{29}$$

 with a_v=15.4941 MeV, a_s=17.9439 MeV, $a_I = 1.7826$ [64] where the surface term is additionally made to vanish at the critical temperature T_C=12 MeV [63]; the Coulomb energy contribution is accounted for in $V_{Coulomb}(C)$ as discussed above; structure effects thoroughly considered by other authors [51] are disregarded because of the relatively high temperatures we are focusing on, but they can be straight-forwardly included;

- in order to avoid multiple counting of the free nucleons, already considered in the uniform background, the clusters should have $Z \geq 2$; this arbitrary limit may be replaced by $A > 1$, such as to allow also for ^{2}H and ^{3}H, but this choice is not expected to be important for the presently considered quantities;

- no limit is imposed for the largest cluster which, in principle, may reach the total system size; given the fact that the fragment mass partition enters in Eq. (16) not only in the translational energy factor and binding energy, but also in the calculations of excluded volume and Coulomb energy, we expect it to play a dramatic role in the limit of low temperatures and densities close to ρ_0;

- to allow creation of exotic species, there is no restriction for the neutron/proton composition; a cluster is allowed to exist as soon as $B(A,Z) > 0$;

- cluster internal excitation energy ϵ is upper limited by the cluster binding energy and the corresponding level density is of Fermi-gas type with cut-off correction [65],

$$\rho(\epsilon) = \frac{\sqrt{\pi}}{12a^{1/4}\epsilon^{5/4}}\ \exp(2\sqrt{a\epsilon})\ \exp(-\epsilon/\tau),\tag{30}$$

 with $a = 0.114A + 0.098A^{2/3}$ MeV^{-1} and τ=9 MeV.

The phase diagram of clusterized stellar matter can be inferred from the bimodal behavior of the total particle number in the grancanonical ensemble [63]. This model presents a first-order liquid-gas phase transition similar to the case of uniform nuclear matter, but contrary to the latter it is never unstable. The two phase diagrams are compared for T=1.6 and 5 MeV in Figs. 1 and, respectively, 2. Fig. 3 presents exclusively the phase diagram of neutral uniform matter at T=10 MeV, as this temperature is supra-critical for the clusterized matter.

We can see that the thermodynamics of a clusterized system is very different from the one of neutral nuclear matter in the mean field approximation, even though the employed effective interaction parameters are typically tuned on the same experimentally accessible observables of cold nuclei close to saturation density, which are implemented in the cluster energy functional. As a consequence, the two phase diagrams are only compatible at low temperatures and at densities close to saturation.

The extension of the coexistence region in density and temperature is noticeably reduced for clusterized matter. This effect is partially not physical. Indeed the numerical procedure adopted for estimating Eq. (16) implies that clusterized matter results depend on the system size for the lowest densities: the lowest accessible density is determined by the chosen finite volume and the minimum allowed cluster size (A_{min}) eventually multiplied by the minimum allowed number of clusters (N_{min}). Clusterized matter phase diagrams considered in this section have been obtained working within a cell of volume $V = 2.9 \cdot 10^4$ fm^3. If $N_{min} = 1$ and $A_{min} = 3$, the lowest accessible density $\rho_{min} = N_{min} A_{min}/V$ is of the order $1.1 \cdot 10^{-4}$ fm^{-3}, which implies that no point below this limit is present. Actually this value is even higher as for numerical efficiency purposes the minimum allowed cluster number is larger than 1.

By consequence, the low density limits of the coexistence zone have to be considered as a numerical artifact. To have trustable predictions at lower densities, the simulation volume will have to be increased in future calculations. Conversely the shrinking of the coexistence zone with increasing temperature and asymmetry is a physical effect.

For a given baryonic density and temperature, we can also see that coexisting phases of clusterized matter are much more isospin symmetric with respect to the ones of the uniform matter, even if the energetics of the two systems corresponds to compatible values for the symmetry energy. This can be physically understood from the fact that higher densities are locally explored if a system is clusterized, and the symmetry energy is an increasing function of density.

Concerning the reduction of the limiting temperature in the clusterized system, this is understood as a cumulated effect of Coulomb and cluster center of mass translational degrees of freedom, which are not accounted for in the homogeneous nuclear matter calculation [63].

These general observations already show the importance of properly accounting for the cluster properties of matter, even if one is only interested in global integrated thermodynamic quantities as equations of state.

From the $\mu_p - \mu_n$ representation it comes out that the coexistence line of the clusterized matter is embedded in the spinodal region of the uniform matter, and shifted towards higher values of μ respect to the coexistence of nuclear matter, that is it corresponds to the low density part of the spinodal region of homogeneous matter. This fact, together of the absence of instability of the clusterized system, is already an indication that the homogeneous matter instability is effectively cured by accounting for the possibility of cluster formation, as we will develop in the next section. In the end, we mention that the phase diagram of clusterized matter might slightly change while modifying cluster properties.

3. The mixture properties

In the previous section we have examined the thermodynamics of purely uniform and purely clusterized nuclear systems. In the physical situation of supernovae and proto-neutron star matter it is clear that these two components have to be simultaneously present, and the question arises of how describing their mutual equilibrium conditions. In many past works [17, 19, 20, 51, 66], the evolution of clusterized matter towards homogeneous matter at high density was described as a first-order phase transition, governed by Gibbs or Maxwell equilibrium rules. The simultaneous presence in the Wigner-Seitz cell of localized clusters and homogeneously distributed free protons and neutrons in the nucleonic drip region is then also depicted as a manifestation of the same first order transition, though corrected by surface and Coulomb effects arising from the finite size of the cell.

However, as we discuss now, the proper way of treating density inhomogeneities occurring at a microscopic (femtometer scale) level is the concept of a gas mixture, if the coexisting components (here: nucleons and fragments) are non-interacting. If interaction effects arising from the excluded volume are included, we show that such a mixture naturally produces a continuous (second order) transition to uniform matter at densities close to saturation.

Restricting for the moment to the baryonic sector, the thermodynamics of a system with two conserved charges ρ_n and ρ_p is a two-dimensional problem. The other charges do not affect the thermodynamics at the baryonic level because they are not coupled to the baryons (see Eq. (1)). The net electron density is coupled to the proton density through the electromagnetic interaction, but this does not imply an additional degree of freedom as charge neutrality imposes $\rho_p = \rho_e$. This two-dimensional problem can be easily taggled if we switch from the grancanonical ensemble, where all the intensive parameters are constrained and the densities can freely vary, to a statistical ensemble where one single extensive observable (i.e. a single density) is free to fluctuate [53]. In our two-dimensional problem, two
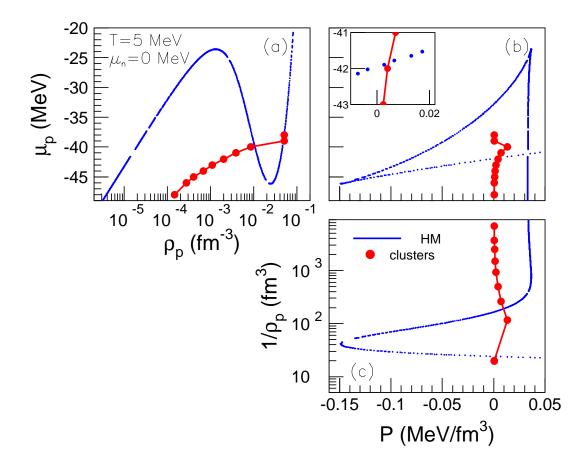
FIG. 4: (Color online) Properties of the uniform (solid lines) and net-charge neutralized clusterized (solid circles connected by lines) matter at $T=5$ MeV and $\mu_n=0$ MeV. Homogeneous matter is described by SKM*.

equivalent possibilities exist, namely the proton-canonical, neutron-grancanonical ensemble where the thermodynamic potential is Legendre transformed to its conjugated extensive variable ρ_p,

$$
\begin{aligned}
s_{pc}\left(\beta, \beta\mu_n, \rho_p\right) & = \frac{1}{V}\bar{S}\left[\beta, -\beta\mu_n\right] \\
& = \frac{1}{V}\ln\mathcal{Z}_{gc}(\beta, \beta\mu_n, \beta\mu_p) - \beta\mu_p\rho_p,
\end{aligned}
\tag{31}
$$

and the neutron-canonical, proton-grancanonical ensemble described by the thermodynamic potential,

$$
\begin{aligned}
s_{nc}\left(\beta, \rho_n, \beta\mu_p\right) & = \frac{1}{V}\bar{S}\left[\beta, -\beta\mu_p\right] \\
& = \frac{1}{V}\ln\mathcal{Z}_{gc}(\beta, \beta\mu_n, \beta\mu_p) - \beta\mu_n\rho_n.
\end{aligned}
\tag{32}
$$

We now come to illustrate the way of mixing clusters and homogeneous matter and the differences between such mixture and a possible phase coexistence which would be associated to a first-order phase transition. Fig. 4 shows the equations of state $\mu_p(\rho_p)$ and $P(1/\rho_p)$ for the proton-canonical ensemble, as well as the functional relation between the two intensive parameters μ_p and P for the uniform (solid lines) and clusterized (solid circles connected by lines) matter at $T=5$ MeV and a representative neutron chemical potential $\mu_n=0$ MeV. The clusterized system is confined within a volume $V = 2.9 \cdot 10^4$ fm^3.

The back-bendings of $\mu_p(\rho_p)|_{(HM)}$ and $P(1/\rho_p)|_{(HM)}$ and the tilting shape of $\mu_p(P)|_{(HM)}$ indicate that in the considered μ_p range uniform matter, if it would exist alone, would be unstable against phase separation.
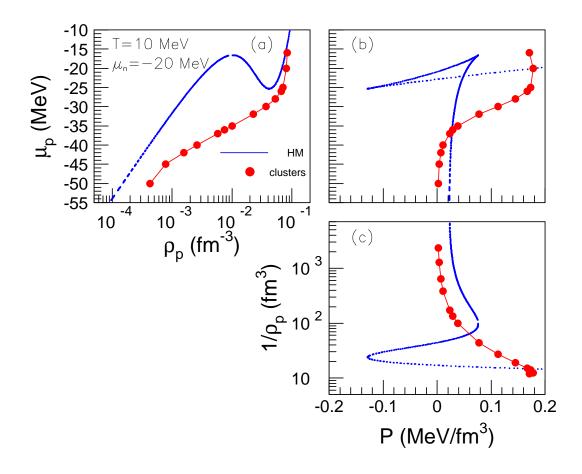
FIG. 5: (Color online) The same as in Fig. 4 for $T=10$ MeV and $\mu_n = -20$ MeV.

If we consider that, at the microscopic scale of the Wigner-Seitz cell, clusters and free nucleons may be simultaneously present, as expected from the phenomenon of neutron drip, then the statistical equilibrium conditions read:

$$\mu_p^{(HM)} = \mu_p^{(cl)} \; ; \; \mu_n^{(HM)} = \mu_n^{(cl)} \; ; \; T^{(HM)} = T^{(cl)} \; ; \; p^{(bar)} = p^{(HM)} w_{HM} + p^{(cl)} w_{cl}, \quad (33)$$

where w_{HM} and w_{cl} measure the volume fractions associated to the homogeneous matter and clusters,

$$w_{HM} = (V - v_{cl}) / V,$$
$$w_{cl} = \left(V - v_0 \left(\rho_n^{(HM)} + \rho_p^{(HM)} \right) (V - v_{cl}) \right) / V, \quad (34)$$

with v_0 standing for the intrinsic volume of a nucleon calculated such as $v_0 = 1/\rho_0$ and $v_{cl} = v_0 \sum_{i=1}^{N_C} A_i$ representing the summed-up clusters intrinsic volumes.

Let us denote by $\mu_{p(H)}^{(HM)}$ and $\mu_{p(L)}^{(HM)}$ the proton chemical potentials corresponding to the limits of the spinodal region of homogeneous matter. For $\mu_p < \mu_{p(L)}^{(HM)} \approx -46$ MeV, there will be one single low density solution of uniform matter which can constitute a mixture at thermal equilibrium with clusterized matter according to Eqs. (33) and which, for sufficiently small values of μ_p, may differ by orders of magnitude from the density of clusters. For $\mu_{p(L)}^{(HM)} < \mu_p < \mu_{p(H)}^{(HM)}$, three different density states of uniform matter can exist in equilibrium with the single solution of clusterized matter, leading to three different mixtures corresponding to the same chemical potentials but different total density, chemical composition and pressure. It is important to stress that these three uniform matter solutions may all lead to thermodynamically stable mixtures, as the stability properties of the entropy has to be examined after

adding all the different matter components. This is at variance with the case of normal nuclear matter, where only one solution out of the three corresponds to a thermodynamically stable state, while the other two are respectively metastable and unstable. For $\mu_p > \mu_{p(H)}^{(HM)} \approx -24 MeV$ the thermodynamic condition is in principle the same as for high and negative chemical potentials. Since however the sum of the two densities corresponding to homogeneous and clusterized matter exceeds ρ_0, the situation goes beyond the applicability domain of the present model and is, thus, devoid of interest.

Given that one of the purposes of our paper is to address the unhomogeneous (crust) - homogeneous (core) transition, it is possible now to anticipate that for these two representative temperatures T=1.6 and 5 MeV this will take place when, following a constant proton fraction trajectory, the uniform matter state will not correspond anymore to the low density, but rather to the high density solution.

At higher temperatures the situation is slightly different as shown by Fig. 5, which shows the same quantities plotted in Fig. 4, for a representative neutron chemical potential at $T = 10$ MeV. In this case, in the relatively narrow chemical potential region where three different homogeneous matter macrostates are found, the corresponding cluster states are always at high density close to saturation. Then, the only mixture solution not overcoming ρ_0 is the one given by the low density solution for uniform matter. At this temperature then, the transition to homogeneous matter does not occur as an increasing proportion of homogeneous matter that becomes abruptly dominant in the mixture as we have just seen at lower temperatures, but rather as an increasing size of the largest cluster which abruptly starts to fill the whole available volume. The two transition mechanisms are physically very close to each other: an infinitely large cluster has the same energetic and entropic properties of homogeneous matter at saturation density, provided the parameters of the effective interaction are compatible with the cluster energy parameters.

Since the thermodynamic potential of the mixture can be expressed as the sum of the thermodynamic potentials corresponding to each sub-system:

$$G^{(bar)}(\beta, \beta\mu_n, \beta\mu_p, V) = G^{(cl)}(\beta, \beta\mu_n, \beta\mu_p, V) + G^{(HM)}(\beta, \beta\mu_n, \beta\mu_p, V), \tag{35}$$

the total neutron and proton density of the mixture is obtained by summing up the corresponding particle numbers,

$$\begin{aligned}
N_{n,p} &= \left(\frac{\partial G^{(cl)}}{\partial(\beta\mu_{n,p})} + \frac{\partial G^{(HM)}}{\partial(\beta\mu_{n,p})} \right) |_{\beta, \beta\mu_{p,n}, V} \\
&= N_{n,p}^{(cl)} + N_{n,p}^{(HM)},
\end{aligned} \tag{36}$$

with the extra condition that nucleons cannot be found in the space occupied by the clusters and vice-versa.

The densities then result:

$$\begin{aligned}
\rho_{n,p} &= \frac{N_{n,p}}{V} \\
&= \frac{N_{n,p}^{(cl)}}{V - v_0\left(\rho_n^{(HM)} + \rho_p^{(HM)}\right)(V - v_{cl})} \cdot \frac{V - v_0\left(\rho_n^{(HM)} + \rho_p^{(HM)}\right)(V - v_{cl})}{V} \\
&\quad + \frac{N_{n,p}^{(HM)}}{V - v_{cl}} \cdot \frac{V - v_{cl}}{V} \\
&= \frac{N_{n,p}^{(cl)}}{V - v_0\left(\rho_n^{(HM)} + \rho_p^{(HM)}\right)(V - v_{cl})} \cdot w_{cl} + \frac{N_{n,p}^{(HM)}}{V - v_{cl}} \cdot w_{HM}.
\end{aligned} \tag{37}$$

The excluded volume correction plays a sizeable role only in the vicinity of ρ_0, and is in particular responsible for the un-homogeneous - homogeneous matter transition at high temperature. More precisely, pure homogeneous nuclear matter phase occurs if $\left(\rho_n^{(HM)} + \rho_p^{(HM)}\right) > \rho_0$ and, respectively, $(V - v_{cl}) \searrow 0$.

The equation of state and constrained entropy of the mixture for (T=5 MeV, $\mu_n = 0$ MeV) and (T=10 MeV, μ_n=-20 MeV) are indicated by circles in Figs. 6 and 7. We can see that the simultaneous presence of the two components constitutes always an entropy gain respect to both purely homogeneous and purely clusterized matter, and corresponds therefore always to the equilibrium solution.

At the lowest temperature the μ_p versus ρ_p equation of state is bivalued in a given density domain. This can be understood as follows. At temperatures low enough that the cluster component shows a liquid-gas transition, which can be recognized from the plateau in the $\mu_p(\rho_p)$ relation at constant μ_n, two very different cluster-matter mixtures

can be obtained from Eqs. (33) and (37) at the same total density but different chemical potentials. These two possible mixtures correspond to a homogeneous matter solution lying inside the spinodal combined respectively to a low density-low chemical potential cluster solution (stars in Fig. 6), or to a higher density-higher chemical potential solution. Since these two possibilities correspond to the same total density, the equilibrium solution will be the one maximizing the associated entropy. It comes out that the lowest chemical potential solution always correspond to a negative total pressure for the mixture, while the pressure associated to the highest chemical potential solution is always positive, meaning that the entropy is higher (see the inset in Fig. 6).

The states denoted by stars in Fig. 6 are therefore unstable or metastable and will not be further considered. The presence of such multiple solutions in this density and temperature domain may be an indication that some degrees of freedom are missing in the model and cluster deformations should be added in this region where pasta structures are expected [11–14].

To summarize, we have modelised the simultaneous presence of free nucleons and light and heavy nuclei as two independent components which are allowed to exchange particles and energy following the laws of statistical equilibrium, and whose proportions are further determined by the geometrical constraint given by the excluded volume.

This means that the densities will have different values in each sub-system and that the partial pressures will be also different, following Eqs. (33) and (37).

The chemical potential equality between the two components insures the global maximization of the total entropy of the mixture. As a result, a smooth decreasing weight of the cluster component is first observed with increasing density, followed by a successive smooth but steeper decrease as density approaches ρ_0. This last result can be intuitively understood from the simple physical fact that when density increases, the space accessible to a clusterized system decreases, and so does the effective number of degrees of freedom. As we will discuss in greater detail in the following, this smooth behavior of the mixture does in no way imply that the crust-core transition is smooth. Indeed because of the characteristic backbending behavior of the homogeneous matter equation of state, which reflects the well-known instability respect to spontaneous density fluctuations, the density content of the homogeneous component can discontinuously change as a function of the chemical potential.

4. Mixture versus phase coexistence

The crust-core transition of a cold neutron star is often [17–20] depicted as a first-order transition from a solid phase of nuclei on a Wigner lattice to a liquid phase of homogeneous nuclear matter. By continuity, a similar phenomenology is thought to occur at the finite temperature and more isospin symmetric conditions involved in supernova matter [23, 51].

This hypothesis arises from essentially two considerations that we now turn to examine:

- The intermediate configuration between the solid crust and the liquid core, namely finite nuclei immersed in an homogeneous neutron background, intuitively resembles to a coexistence between a clustered and a homogeneous baryonic phase.

- Normal nuclear matter is known to present an instability respect to cluster formation and phase separation. This spinodal instability is associated to a first-order transition. By continuity the same is expected in the baryonic part of stellar matter.

Let us first concentrate on the first statement. As we have already mentioned, the simultaneous presence of two different states characterized by a different average value for an order parameter (here: baryonic density) constitutes a phase coexistence if and only if the order parameter fluctuations (here: density inhomogeneities) occur on a length scale which is macrosocopic respect to the range of the interaction (here: much larger than the femtometer scale of typical nuclei size). This condition on macroscopic scales is necessary because the Gibbs construction neglects the interface energy and entropy, which is essential to describe thermodynamics of finite systems [69]. Since this is clearly not the case in stellar matter, surface and Coulomb terms are sometimes added [23] to approximately account for finite-size corrections. However we have shown in the last section that the modelization of a microscopic mixture between clusters and homogeneous matter is also a way to describe the intermediate configurations between core and crust. Therefore we may ask if the two modelizations of phase mixture and phase coexistence are equivalent or at least lead to equivalent results for the observables of interest.

To clarify this point, let us consider homogeneous and clusterized matter as two different possible phases for stellar matter which may coexist at a first-order transition point. The advantage of working with an hybrid ensemble as the proton-canonical ensemble defined above, is that the two-dimensional tangent construction implied by Gibbs
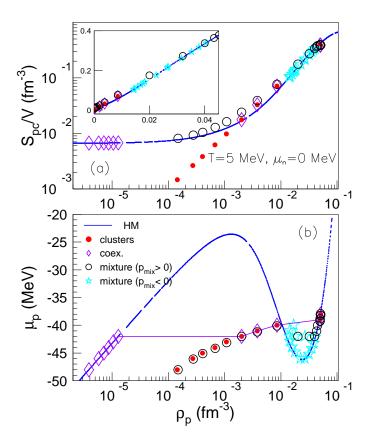
FIG. 6: (Color online) μ_p versus ρ_p (bottom) and $\bar{S}[\beta, -\beta\mu_n]/V$ versus ρ_p (top) for the homogeneous-clusterized matter coexistence (open diamonds) and mixture (open circles if $p_{mix} > 0$ and stars if $p_{mix} < 0$) at T=5 MeV along the constant $\mu_n = 0$ MeV path. The homogeneous matter and net-charge neutralized cluster matter curves are plotted with solid line and, respectively, small solid symbols.

conditions in a multi-component first-order phase transition [67, 68] is reduced to a simple one-dimensional Maxwell construction on the unique free extensive variable [53]. It is important to stress that this procedure is just a technical simplification and the obtained equilibrium is exactly identical to the usual two-dimensional Gibbs construction in the grancanonical ensemble. This construction in a Legendre-transformed potential should not be confused with a Maxwell construction on the $p(\rho)$ equation of state performed on trajectories characterized by constant proton fractions $Y_p = \rho_p/\rho$, which is currently used in the literature [23] and has no physical justification. Indeed in a first-order phase transition in a two-component system the chemical composition of the two coexisting phases is never the same and the total pressure is a monotonically increasing function of the total density [67]. This means that a Maxwell construction on $p(\rho)$ at constant Y_p does not give the correct Gibbs equilibrium.

The inset in the right upper panel of Fig. 4 shows that for the representative (T, μ_n) choice of the figure the two components are found at the same value of proton chemical potential and pressure in a single point located at $(P^t, \mu_p^t) \approx (0.005 \text{ MeV/fm}^3 , -41.8 \text{ MeV})$. Only at this point the Gibbs equilibrium rule for coexisting phases is fulfilled,

$$\mu_p^{(HM)} = \mu_p^{(cl)} \; ; \; \mu_n^{(HM)} = \mu_n^{(cl)} \; ; \; T^{(HM)} = T^{(cl)} \; ; \; p^{(HM)} = p^{(cl)}. \tag{38}$$

As it can be seen in Fig. 4, at this point the density of the two components differs of more than two orders of magnitude. If clusters and homogeneous matter could be viewed as two different phases for stellar matter, the global system would be composed of homogeneous matter only for $\mu_p < \mu_p^t$, and of clusters only for $\mu_p > \mu_p^t$, with a discontinuous (first-order) transition at the transition point $(P^t(T, \mu_n), \mu_p^t(T, \mu_n))$. The effect of this construction on the equation of state is shown on Fig. 6 by the open diamonds. Within the picture of a first-order phase transition, stellar matter at the chosen representative (T, μ_n) point would be homogeneous at low density up to $\rho_p = \rho_p^m$, with $\rho_p^m \approx 1.2 \cdot 10^{-5}$ fm^{-3}; for intermediate densities $\rho_p^m \leq \rho_p \leq \rho_p^M$, with $\rho_p^M \approx 2 \cdot 10^{-3}$ fm^{-3}, it would be a combination
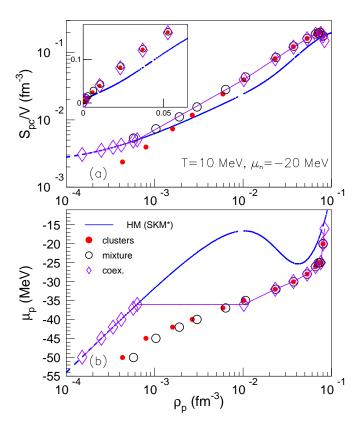
FIG. 7: (Color online) The same as in Fig. 6 for T=10 MeV and $\mu_n = -20$ MeV.

of matter and clusters varying in linear proportions; and at high density $\rho_p \geq \rho_p^M$ it would be solely composed of clusters, which would extend over the whole volume at the highest densities. As we can see, this equation of state is very different from the physically meaningful one corresponding to a continuous mixture of matter and clusters over the whole density domain. However, the two models lead to an almost equivalent entropy, as it is shown by the upper part of Fig. 6.

Similar considerations apply at other temperatures and chemical potentials. As a second example, Fig. 7 compares the properties of the mixture with the ones of an hypothetical first-order transition for $T = 10$ MeV and $\mu_n = -20$ MeV, the same thermodynamic conditions as in Fig. 5. Only within the mixture picture free protons in weak proportions are present in the matter, as it is physically expected. An inspection of the behavior of the constrained entropy at this high temperature (higher part of Fig. 7) clearly shows that the continuous mixture of nucleons and clusters not only correctly recovers the homogeneous matter properties at high density, but is also very effective in compensating the mean-field instability of homogeneous matter at lower densities, leading to a concave entropy over the whole density range (see the inset in the upper panel). Thus the usual argument that a phase coexistence would be needed to maximize the entropy and cure the convexity anomaly of the entropy cannot be applied: the same entropic gain is obtained considering a continuous mixture, without applying an artificial construction which neglects all finite-size effects.

We note by passing that at high temperature there are two (p, μ_p) points satisfying the Gibbs conditions Eq. (38) for a given value of μ_n (see Fig. 5). However at the second point at high pressure the two components correspond to almost the same density. Making a mixture or a phase coexistence does not therefore produce any sensitive difference in the equation of state (lower part of Fig. 7) in this density region.

The matter composition obtained with a continuous mixture is compared to the one corresponding to a discontinuous transition obtained with the Gibbs construction in Fig. 8. We can see, together with the different behavior of the equation of state, that the predictions for the average cluster size and cluster multiplicity show quantitative differences. It is difficult to know a priori the consequence of such altogether slight differences on the macroscopic modelization of supernova matter, and we cannot exclude that the use of a mixture equation of state would not be
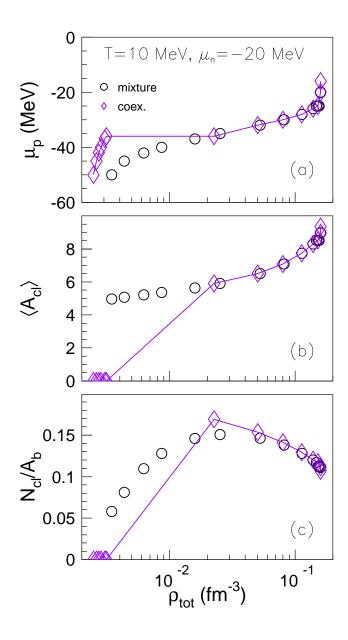
FIG. 8: (Color online) Mixture versus coexistence for T=10 MeV and $\mu_n = -20$ MeV. Up: μ_p versus ρ_{tot}; Middle: average mass of a cluster versus ρ_{tot}; Bottom: average cluster number per total baryon number versus ρ_{tot}.

really distinguishable from the currently used approximations employing first-order phase transitions. Even if this would be the case, the discontinuities in all thermodynamic quantities implied by these artificial first-order transitions lead to numerical instabilities in supernova codes [70] which are difficult to handle, and which could be avoided using continuous equations of state.

To defend the possibility of a first-order crust-core transition, one may argue that the behavior of the entropy as a function of the density shown in Figs. 6 and 7 is certainly model dependent, and that in general residual convexities could still be present after considering the mixture of nucleons and clusters, especially at the lowest temperatures. Such convexities would represent residual instabilities and should then be cured with a Gibbs construction, leading again to a first-order phase transition from a low-density, cluster dominated mixture to a high density, matter dominated mixture as in the usual representation of a neutron star. Such an instability is known to be present in homogeneous nuclear matter, as shown by the back-bendings of Figs. 4 and 5, and it may well survive if clusterization was allowed in a microscopic way [50] going beyond the mean-field approximation in a microscopically consistent way.
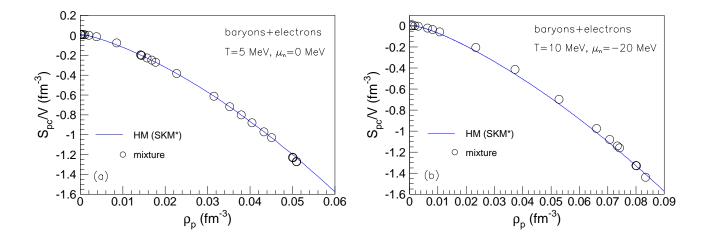
FIG. 9: (Color online) Constrained entropy for the ensemble baryons plus electrons at T=5 MeV along the constant $\mu_n = 0$ MeV path (left panel) and at T=10 MeV and $\mu_n = -20$ MeV (right panels) for the homogeneous matter (full line) and the mixture of matter and clusters (open circles).

The argument exposed above is the second argument which can be invoked to justify a discontinuous transition, which was mentioned at the beginning of this section, and that we now come to discuss.

It is certainly correct that our model depicting the simultaneous presence of nucleons and clusters as a non-interacting mixture of two different components associated to completely independent degrees of freedom and self-energies is highly schematic, and improvements are in order.

In particular the way the excluded volume is parametrized has an influence on the quantitative balance between nucleons and clusters, with a possible consequence on the precise location of the transition which is not completely under control.

Fully self-consistent treatments of the quantal many-body problem at finite temperature as in Refs. [47–50], including the possibility of self-consistent clustering at low densities are extremely promising, and will in the long run provide a much better description of stellar matter than the phenomenological model proposed here. Concerning the issue of the order of the transition however, we believe that the availability of such sophisticated calculations would not modify our conclusions. Indeed, as we have already stated, the thermodynamic stability has to be checked on the global thermodynamic potential Eq. (1), after all the different constituents are added up. If gammas and neutrinos are completely decoupled from the baryonic sector, this is not true concerning electrons and positrons because of the neutrality constraint $\rho_p = \rho_e$. Because of this, the properties of the electron free energy will influence the convexity properties of the baryonic entropy as a function of the density.

Fig. 9 shows the thermodynamic potential of the proton-canonical, neutron-grancanonical ensemble in the same thermodynamic conditions as in Figs. 6 and 7, including the contributions of electrons (detailed in the next section) and explicitly including the neutrality constraint

$$s_{pc}^{tot}(\beta, \beta\mu_n, \rho_p) = \frac{1}{V} \ln \mathcal{Z}_{gc}^{(cl)}(\beta, \beta\mu_n, \beta\mu_p) + \frac{1}{V} \ln \mathcal{Z}_{gc}^{(HM)}(\beta, \beta\mu_n, \beta\mu_p) + \frac{1}{V} \ln \mathcal{Z}_{(\beta, \beta\mu_e)}^{(el)} - \beta(\mu_p + \mu_e)\rho_p, \qquad (39)$$

We can see that taking into account the presence of clusters has virtually no effect on the convexity of the global entropy, which is largely dominated by the convexity properties of the electron thermodynamic potential. Since this latter is highly concave, whatever the treatment of the baryonic sector, the global entropy will stay concave in the whole density domain. The effect of the electrons is thus to compensate the instability of nuclear matter and quench the possibility of a first-order phase transition.

This result can be physically understood [16, 71]: because of the low electron mass, the electron gas is much more incompressible than the nuclear component. A fluctuation in the baryonic density creates a fluctuation in the charge density, which because of the neutrality constraint implies a fluctuation in the net electron density. Such fluctuations are naturally present in the length scale of the Wigner-Seitz cell, and are at the origin of the electrostatic interaction energy which is non-zero even if the system is neutral, see Eq. (25). However these fluctuations cannot extend over

macroscopic lengths because they would imply macroscopic electron inhomogeneities, which are contrasted by the high electron incompressibility.

To conclude, phases of different global baryon density cannot exist in stellar matter if baryonic matter is constituted of heavy particles as nucleons and clusters, as it is the case at the densities of interest in the present paper. Since this statement is valid for all chemical potentials and temperatures, including $T = 0$, we conclude that the crust-core phase transition cannot be of first-order at any temperature.

B. Leptons and photons

In the temperature and density domains relevant for this paper, $T > 1$ MeV and $\rho > 10^6$ g $\cdot$ cm^{-3}, leptons (electrons and neutrinos) are relativistic, in particle-antiparticle pair equilibrium and in thermal equilibrium with nuclear matter [17, 23].

Given that the net charge of the electron gas (that is the number of electrons minus the number of positrons) has to neutralize the positive charge of protons in uniform and clusterized matter, the electron chemical potential μ_e is determined by the equality among the electron density, calculated in the relativistic Fermi gas model, and the proton density,

$$\rho Y_p = \frac{g_e}{6\pi^2} \left(\frac{\mu_e}{\hbar c}\right)^3 \left[1 + \frac{1}{\mu_e^2} \left(\pi^2 T^2 - \frac{3}{2} m_e^2 c^4\right)\right], \tag{40}$$

where ρ represents the baryon density, $g_e = 2$ is the spin degeneracy and m_e is the rest mass.

The electron gas pressure, entropy and energy densities are functions of T and μ_e and their expressions are the following,

$$p^{(el)} = \frac{g_e \mu_e}{24\pi^2} \left(\frac{\mu_e}{\hbar c}\right)^3 \left[1 + \frac{1}{\mu_e^2} \left(2\pi^2 T^2 - 3 m_e^2 c^4\right) + \frac{\pi^2 T^2}{\mu_e^4} \left(\frac{7}{15}\pi^2 T^2 - \frac{1}{2} m_e^2 c^4\right)\right], \tag{41}$$

$$s^{(el)} = \frac{g_e T \mu_e^2}{6\rho (\hbar c)^3} \left[1 + \frac{1}{\mu_e^2} \left(\frac{7}{15}\pi^2 T^2 - \frac{1}{2} m_e^2 c^4\right)\right], \tag{42}$$

and, respectively,

$$e^{(el)} = \frac{g_e \mu_e}{8\pi^2 \rho} \left(\frac{\mu_e}{\hbar c}\right)^3 \left[1 + \frac{1}{\mu_e^2} \left(2\pi^2 T^2 - m_e^2 c^4\right) + \frac{\pi^2 T^2}{\mu_e^4} \left(\frac{7}{15}\pi^2 T^2 - \frac{1}{2} m_e^2 c^4\right)\right]. \tag{43}$$

Neutrinos also form a relativistic Fermi gas in pair equilibrium and thermal equilibrium with nuclear matter. This means that Eqs. (40, 41, 42 and 43) with $m_\nu = 0$ and $g_\nu = 1$ instead of m_e and g_e describe their density, pressure, entropy and energy densities. Under the β-equilibrium hypothesis, neutrinos chemical potential is dictated by the chemical potential of neutrons, protons and electrons,

$$\left(\mu_p + m_p c^2\right) + \left(\mu_e + m_e c^2\right) = \left(\mu_n + m_n c^2\right) + \mu_\nu. \tag{44}$$

If not explicitly mentioned otherwise (section III.C), all over this paper we shall work out of β-equilibrium. Neutrinos contribution to the total energy, entropy and pressure will be disregarded, as well. The motivation of this choice is that equilibration with respect to weak interaction is often not achieved over the time scales of many astrophysical phenomena, but we will discuss this point further in section III.C.

Photons are assumed to be in thermal equilibrium with the other star ingredients and their pressure, entropy and energy densities are,

$$p^{(\gamma)} = \frac{\pi^2 T^4}{45 (\hbar c)^3}, \tag{45}$$

$$s^{(\gamma)} = \frac{4 p^{(\gamma)}}{\rho T}, \tag{46}$$

and, respectively,

$$e^{(\gamma)} = \frac{3 p^{(\gamma)}}{\rho}. \tag{47}$$

III. STAR MATTER RELEVANT RESULTS

A. Constant chemical potential paths

In the evolution of supernovae explosions, nuclear composition plays an extremely important role. First of all, isotopic abundances in the light and medium mass region influence nucleosynthesis via r-, rp- and photodisintegration processes. Then, nuclei with masses larger than 40-60 determine the rate of electron capture [33, 34], the most important weak nuclear interaction in the dynamics of stellar core collapse and bounce, responsible for the neutron enrichment of baryonic matter and neutrino emission. On the other hand, nuclei absorb energy via internal excitation making the increase in temperature and pressure during star collapse be less strong than in the case of a uniform nucleon gas [27]. Nuclei influence also the maximum density reached during the collapse. In the absence of nuclei the collapse stops before reaching ρ_0, while the limiting value is larger than ρ_0 if nuclei are present [28]. Finally, by dissociation under the shock wave, nuclear composition affects the shock propagation [30].

Under this perspective, it is obvious that realistic star matter equations of state require accurate treatment of the nuclear statistical equilibrium. Working within the single nucleus approximation (SNA), the first generation models [17, 23] do not offer a satisfactory description of nuclear miscellanea and may be to some extent responsible for the failure of present supernovae simulations to produce explosions, even if realistic neutrino transport[72] and convective instabilities in multi-dimensional hydrodynamics[73] are probably the key ingredient of a successful explosion of highly massive cores. Most recent statistical models [42, 44, 51] fix this inconvenience by working in a grancanonical approximation (GCA) which allows for continuous distributions in the nuclear cluster mass and charge. This means that practically everywhere in the temperature - density domain, the 'cluster gas' may contain a variety of nuclei of very different sizes. In our model these, additionally, may change from one configuration to the other, meaning that the composition fluctuation is also accounted for.

To understand the correlation between the thermodynamic properties and the matter composition obtained with our model, Fig. 10 presents the evolution with density of the average cluster size and isotopic composition at the three temperatures $T = 1.6, 5, 10$ MeV analyzed before, and for some chosen characteristic values of the chemical potentials, in comparison to the Lattimer-Swesty (LS) model employing the single nucleus approximation (SNA) [74]. As a technical detail, we mention that at T=1.6 and 5 MeV the clusterized matter was treated within a canonical-constant Z ensemble, while a grand-canonical one was employed at T=10 MeV. In all considered cases, the cell volume spanned the domain $1.9 \cdot 10^4 - 1.4 \cdot 10^8$ fm^3.

The left part of the figure shows the evolution with temperature and density of the average cluster size, compared to the single nucleus size of LS, corresponding to the same effective nucleon-nucleon potential, SKM*. The general trend, which is independent of the chosen values of the chemical potential, is an increase with density and a decrease with temperature of the cluster size. This behavior is smooth, even though from the thermodynamic viewpoint at $T = 1.6$ MeV and $T = 5$ MeV the calculation corresponds to the coexistence zone for the cluster component (stars in the left part of Figs. 1 and 2), while $T = 10$ MeV is supercritical for clusters. This smoothness is due to the presence of the homogeneous matter component as a continuous mixture, as we have discussed in Section II.A.3. The only indication of the underlying cluster phase transition can be seen from the fluctuations of the size distribution, indicated by the vertical bars in Fig. 10, which are maximal at $T = 5$ MeV in the middle of the coexistence region as it is well known from multifragmentation studies in finite nuclei [76–78]. The open stars in Fig. 10 denote the unstable or metastable mixture solutions discussed in section II.A.3, obtained when the homogeneous matter component is characterized by a density very similar to the density of the clusters. As we have already mentioned, the presence of these multiple solutions with similar entropy content may be an indication that allowing for pasta-like clusters may provide a higher entropy solution.

Coming to the comparison to LS, the two models nicely agree at low density and temperature, but important differences are seen elsewhere. In the LS model the crust-core transition is a discontinuous (first-order) disappearance of the single heavy cluster which merges at high density and temperature with homogeneous matter: this is why A_{cl} decreases with density at $T = 5$ MeV in LS, and clusters abruptly disappear at the temperature dependent transition points. This is at variance with our calculation, where both components exist, though in very different proportions, in the whole temperature and chemical potentials space.

Considering alpha particles together with the heavy nucleus when discussing the 'cluster component' in the LS case and defining $A_{cl} = (A_{heavy} + 4N_\alpha)/(N_\alpha + 1)$ would not change the situation. The explanation relies on the fact that, for these trajectories, when a heavy cluster exists the number of alpha particles in a cell is negligible.

The right part of Fig. 10 gives the average cluster chemical composition, while the fluctuations of this quantity are given by the vertical bars. We can see that at low temperature (below the cluster limiting point) the isospin
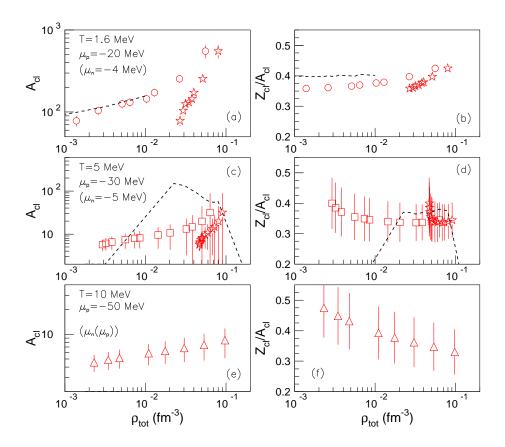
FIG. 10: (Color online) Evolution with total baryonic density of the cluster size (left) and isospin composition (right) along trajectories of constant μ_p for T=1.6, 5 and 10 MeV. Open circles, squares and triangles: predictions of the present model corresponding to a positive total pressure of the mixture $p_{mix} > 0$; open stars: the same as above for a negative total pressure of the mixture $p_{mix} < 0$; dashed lines: Lattimer-Swesty data from Ref. [74].

content of clusters is fairly constant both in our calculation and in the LS model. This is expected, since by definition a trajectory moving inside a coexistence region implies a transformation $\mu_p = \mu_p^{trans}$ =cte and $\mu_n = \mu_n^{trans}$ =cte, that is $<Z>/<A>$=cte. Since a huge part of the density plane at low temperature belongs to the coexistence region if the cluster component is considered alone (see Figs. 1 and 2), the chosen trajectory can span the whole relevant density domain staying inside the coexistence, that is at constant chemical composition. The little deviations observed in our calculation from this constant behavior at high density have to be considered as numerical accidents due to the non-perfect achievement of the thermodynamic limit.

In the case of $T = 10$ MeV, the chemical composition is entirely determined by the chosen transformation and has no specific physical meaning. It is interesting to remark that, except at the lowest temperature, this quantity presents very huge fluctuations that cannot be addressed within the single nucleus approximation SNA.

Changing the chosen chemical potential value obviously modifies the behavior of the chemical composition with density, but does not change our qualitative conclusions.

Fig. 11 displays the characteristics of the Wigner-Seitz cell in terms of baryonic number, proton fraction and linear size, in the same thermodynamic conditions of Fig. 10. The Wigner-Seitz size is defined as the total baryonic mass associated to each fragment,

$$A_{WS} = \frac{\langle \sum_i A_i \rangle}{N_{cl}}, \tag{48}$$

where the sum runs over clusters and free nucleons, and $N_{cl} =< N_C >$ is the average cluster number obtained in the simulation. It is important to stress that the concept of a Wigner-Seitz cell is very different in our approach and in SNA. While in SNA the Wigner-Seitz cell is a primitive cell, *i.e.* the smallest volume element which contains complete information on the infinite system and from which the last one can be built, in GCA we work with an ensemble of tens or hundreds of elementary cells. None of these cells is primitive, as their cluster partitions may differ. Only
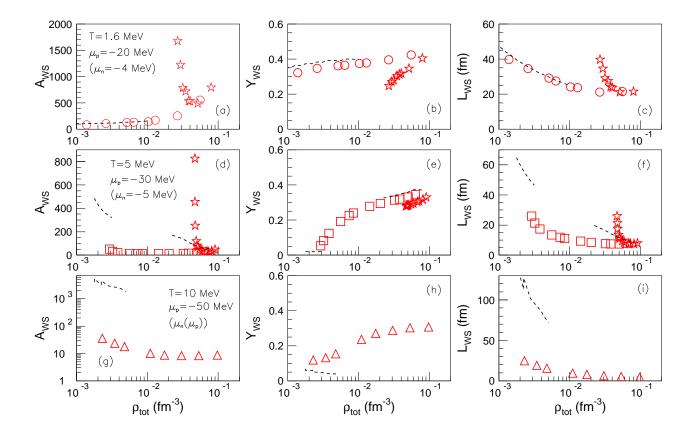
FIG. 11: (Color online) Evolution with total baryonic density of the total baryonic number (left), proton fraction (middle) and linear dimension (right) of the Wigner-Seitz cell for T=1.6, 5 and 10 MeV along trajectories of constant μ_p. Open symbols: predictions of the present model; dashed lines: Lattimer-Swesty data from Ref. [74].

within fluctuations they may be seen as replica of an *average elementary cell*, the counterpart of the Wigner-Seitz cell in SNA.

The decrease of A_{WS} with increasing density, as observed both in LS and in our calculations at high temperature, can be understood as a trivial compression effect, which implies that reducing the volume the matter composition does not drastically change. A different behavior is seen at low temperature, due to the rapid increase of the heaviest cluster size towards the transition to the core.

As before, open stars denote unstable mixture solutions and we cannot exclude that the crust-core transition would be more abrupt if additional degrees of freedom were added in our model at high density. Indeed at the peak a small cluster coexists with a huge quantity of slightly diluted matter. This situation is energetically similar to a very big bubble in a dense $\rho = \rho_0$ medium, but the absence of deformation degrees of freedom may suppress the entropy of such exotic configurations.

Concerning the comparison with the LS model, the two calculations fairly agree only at low temperature. As a general trend, taking into account the whole equilibrium distribution of clusters (GCA) produces smaller fragments (see Fig. 10, left panel) with higher multiplicity respect to the single nucleus SNA approximation. This is in qualitative agreement with other authors findings [42, 44, 51]. The absence of points at intermediate density at $T = 5$ MeV is not an effect of the discontinuous transitions in LS, but is simply due to the fact that LS calculations are performed in discrete Y_p steps, and therefore some points are missing when looking for μ =cte trajectories. The much higher A_{WS} seen in LS calculations at high temperature is due to the fact that no fragments other than alphas are present there in the SNA approximation (see Fig. 10). In this situation ($\rho_{tot} < 3 \cdot 10^{-3}$ fm^{-3} for T=5 MeV and the whole considered total density domain at T=10 MeV), the cell is built around an alpha particle such that the total baryonic mass of a cell becomes,

$$
\begin{aligned}
A_{WS} &= (N_n + N_p + 4N_\alpha)/N_\alpha \\
&= 12 + 4(\omega_n + \omega_p)/\omega_\alpha,
\end{aligned} \tag{49}
$$

where N_n, N_p, N_α and ω_n, ω_p, ω_α denote respectively the number of free neutrons, free protons and alpha particles per unit volume and the corresponding mass fractions. This makes the Wigner-Seitz mass increase because of our definition $A_{tot}/V = A_{WS} N_{cl}/V$.

The global proton fraction of the Wigner-Seitz cell is shown in the middle panels of Fig. 11 as a function of temperature and total density. At the lowest temperature fragments dominate in the global composition, which implies that the behavior of the cell closely follows the behavior of the proton fraction of the clusters shown in Fig. 10. At higher temperature, clusters start to be immersed in a nuclear gas which is neutron rich. As density increases, proton drip becomes allowed slightly increasing the proton fraction of the free nucleons. Since matter dominates over fragments at high density and temperature, Y_{WS} reflects this behavior.

Finally the right part of Fig. 11 shows the average distance among fragments, which can be physically interpreted as the linear size of the Wigner-Seitz cell:

$$L_{WS} = \left(\frac{V}{N_{cl}} \right)^{1/3} . \tag{50}$$

In the case of SNA, at temperatures where the heavy nucleus is not present any more, this quantity is replaced with the average distance among alphas. L_{WS} decreases with density and temperature as expected. Again, only in the thermodynamic conditions where a single massive cluster dominates in the equilibrium distribution (that is: at the lowest temperature) the results agree with the SNA approximation which assumes a single cluster in the whole phase diagram.

B. Results at constant proton fraction

The construction of the phase diagram and mixture properties requires to work in a grancanonical formulation, that is fix the intensive observables T, μ_n and μ_p, or alternatively in a canonical formulation working in terms of T, ρ_n and ρ_p, where ρ_n and ρ_p stand for the total neutron and proton densities, *i.e.* the summed up contributions of uniform and clusterized matter. For the purpose of studying the stability properties of the different phases, hybrid ensembles where only one charge is let free to fluctuate have also been employed.

These variables are however not convenient to use for expressing the equation of state of stellar matter, as the chemical potentials are not measurable and the total baryonic density is of outmost importance for astrophysical applications.

The mostly spread choice is then to work in terms of $(T, \rho$ and $Y_p)$, where $\rho = \rho_n + \rho_p$ is the total baryonic density and $Y_p = \rho_p/\rho$ is the proton fraction. The net charge neutrality requires proton and electron fractions to be equal, $Y_p = Y_e$.

Let us adopt these coordinates and investigate which are the domains of μ_n and μ_p spanned by the total system with two arbitrarily chosen values of Y_p=0.2 and 0.3 if the total density ranges from ρ_0 to $\rho_0/1000$. The results are plotted in Fig. 12 for the same values of temperature considered before, T=1.6, 5 and 10 MeV. Present model predictions (open circles, squares and triangles) are systematically compared to LS predictions [74] (dashed lines). While for $\mu_n(\rho)$ our predictions agree with LS, for $\mu_p(\rho)$ this is true only in the limit of low and medium temperatures. At the highest considered temperature (T=10 MeV) and $\rho > \rho_0/100$ present model predictions differ from the LS ones by few tens of MeV.

This difference between the models can be understood as an effect of the presence of clusters at high temperature implied by our approach. The thin dotted line corresponds to a calculation where the cluster contribution in the mixture is artificially switched off, and the nuclear matter is made out exclusively of free nucleons. Quite remarkably, in this case our calculation agrees with LS predictions, which can be understood knowing that the amount of mass contained in clusters in LS at high temperature is negligible, as we have seen in the previous section. We want to stress that the total entropy of the mixture is always higher than the total entropy of homogeneous matter (see Fig. 7), meaning that our mixture solution is preferred at equilibrium.

Surprisingly, this difference between the models is not seen for the neutron chemical potential (left side of Fig. 12). A very similar behavior was already observed in Ref. [51]. This can be understood from inspection of Fig. 13, which displays the relation between μ_n, μ_p, Y_p and ρ at $T = 10$ MeV for the homogeneous matter and clusterized component.

Let us look at the homogeneous matter first. Because of the symmetry properties of the effective interaction, the behavior of $\mu_n(\rho)$ at constant μ_p is the same as the behavior of $\mu_p(\rho)$ at constant μ_n, and shows the characteristic
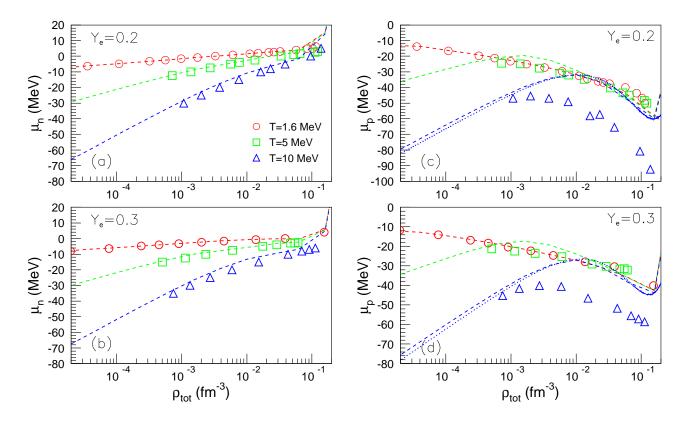
FIG. 12: (Color online) μ_n (left panels) and μ_p (right panels) versus total baryonic density for different values of the constant proton fraction Y_e=0.2, 0.3 and temperature T=1.6, 5 and 10 MeV. Present model predictions are illustrated with open circles (T=1.6 MeV), squares (T=5 MeV) and triangles (T=10 MeV); dashed lines correspond to Lattimer-Swesty results [74]. In both cases the uniform matter component is described by SKM*. The thin dotted line corresponds to the case in which, and T=10 MeV, nuclear matter would exclusively consist out of free nucleons.

back-bending implied by the homogeneous matter instability. Because of that, the behavior of the proton fraction $Y_p(\rho)$ at constant μ_n is also back-bending, and the behavior of $Y_p(\rho)$ at constant μ_p is inverted respect to it. A constant $Y_p = 0.3$ path then explores, as a function of the density, the back-bending region of the iso-μ_p, while an analogous behavior for the iso-μ_n would be seen in the (unphysical) symmetric trajectory $Y_p = 0.7$. As a consequence, μ_p shows a maximum as a function of the density for this low value of the proton fraction while μ_n is a monotonically increasing function, as observed in Fig. 12. Turning to the clusterized component, this latter does not show any instability meaning that the chemical potentials are monotonically increasing functions of the density. Then the behavior of Y_p as a function of the density at constant (neutron or proton) chemical potential is essentially flat, and the net effect is to translate the maximum of μ_p in the constant proton fraction trajectories, while no effect is seen in μ_n because of its monotonic behavior at this low Y_p. This explains the different behavior of the two chemical potentials at constant proton fraction seen in Fig.12.

We now turn to analyze some quantitative predictions of our model concerning both matter composition and equations of state, in thermodynamic conditions which are relevant for supernova matter.

1. Matter composition

Fig. 14 illustrates the total baryonic density dependence of the average fragment mass fraction $< A_{cl} > /A_{WS}$ (left panels), cumulated fragment mass fraction $\sum_{i=1}^{N_C} A_i/A_{WS}$ (middle panels), and average number of clusters per baryonic number (right panels) for the three values of temperature already considered, T=1.6, 5 and 10 MeV, densities ranging from 10^{-5} to 10^{-1} fm^{-3} and Y_p=0.2 and 0.3. LS predictions (dashed lines) correspond to the unique heavy nucleus of SNA whose mass fraction is immediately calculated out of the mass fractions of free neutrons, free protons and alphas, $\omega_{heavy} = 1 - (\omega_n + \omega_p + \omega_\alpha)$ (left panels) and, respectively, summed-up contributions of the heavy nucleus
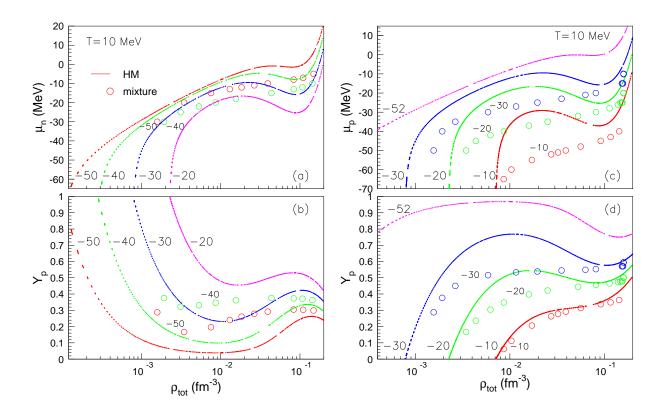
FIG. 13: (Color online) $\mu_{n,p}(\rho)|_{\mu_p,\mu_n}$ (top) and $Y_p(\rho)|_{\mu_p,\mu_n}$ (bottom) curves at T=10 MeV. The values of the constant chemical potentials are expressed in MeV. Solid lines correspond to the homogeneous matter; open circles correspond to the mixture between homogeneous and clusterized matter.

and alpha particles ($\omega_{heavy} + \omega_\alpha$) (middle panels). The fact that alpha particles are considered for LS also when computing N_{cl}/A_{WS} is responsible for the double-humped structure of the corresponding distributions (right panels).

The huge difference between SNA and GCA in what regards A_{cl}/A_{tot} vs. ρ is due to the different acceptations of the cell concept in the two frameworks. As we have already mentioned, contrary to SNA in GCA no primitive cell exists: because of the fluctuations implied by finite temperature, the system cannot be viewed as an infinite number of replicas of a single elementary volume element containing one single cluster.

Quite remarkably, the discrepancies originating from cell fluctuations are to a large extent washed-out when alpha particles are included (middle panels) and SNA and GCA agree much better. However, at $T=5$ MeV and, to a larger extent, at $T=10$ MeV GCA accounts for more mass bound in massive and light nuclei than SNA. This result may be considered a step forward in making numerical simulations of stellar evolution able to reproduce the supernovae explosions. The same qualitative information on cell population is revealed by the cluster number per baryon number depicted in the right panels, for which the maximum deviation is observed at the highest temperature. The bimodal character of the SNA distributions is an artefact of the fact that only two types of nuclei, αs and the heavy nucleus, are allowed to exist, each of them being preferentially produced in another total density domain. A fully microscopic description of nuclear matter composed of neutrons, protons and alpha particles has been recently proposed by Horowitz and Schwenk [75] and relies on the virial expansion of the equation of state. The results corresponding to the density dependence of the cumulated cluster mass fraction $4n_\alpha/(n_n + n_p + 4n_\alpha)$ and average cluster number per baryonic number $n_\alpha/(n_n + n_p + 4n_\alpha)$ are plotted with dot-dashed lines in the middle and, respectively, right panels. The density domains over which this calculation is possible was fixed by the condition of having sub-unitary nucleon fugacities. From a qualitative point of view, our model agrees with HS in the sense that both of them show a smooth behavior of X_{nuclei} and N_{cl}/A_b as a function of ρ. From a quantitative point of view, the absence of nuclei heavier than alpha particles makes HS systematically underestimate, in the density domains where such heavy cluster may exist, the percentage of mass bound in clusters with respect to both present model and LS. On the other hand, in the temperature-density regions where the largest cluster allowed by LS is the alpha particle, there is no clear relation among the predictions of the two models. Thus, at $T=5$ MeV and $\rho \leq 3 \cdot 10^{-3}$ fm^{-3} HS and LS predictions agree perfectly while for $T=10$ MeV and $1 \cdot 10^{-3} \leq \rho \leq 1.8 \cdot 10^{-2}$ fm^{-3} HS results exceed those corresponding to LS.
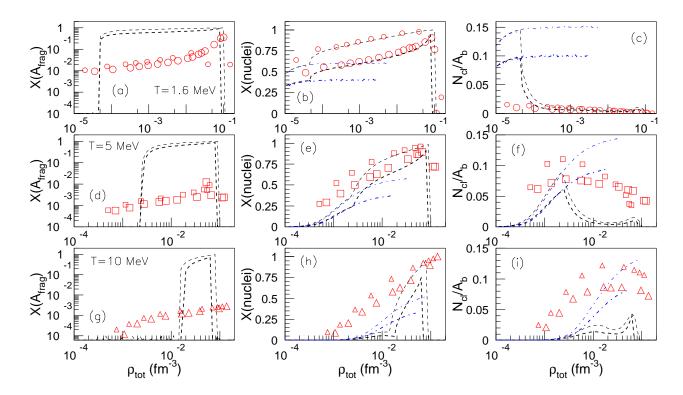
FIG. 14: (Color online) Evolution with total baryonic density of the average fragment mass fraction (left panels), cumulated cluster mass fraction (middle panels) and cluster number per baryonic number (right panels) for T=1.6, 5 and 10 MeV. Large and small open symbols stand for present model predictions corresponding to Y_e=0.2 and, respectively, 0.3; think (Y_e=0.2) and thin (Y_e=0.3) dashed lines illustrate Lattimer-Swesty data from Ref. [74]; think (Y_e=0.2) and thin (Y_e=0.3) dot-dashed lines correspond to the Horowitz-Schwenk results based on the virial expansion of the equation of state [75].

2. Homogeneous-inhomogeneous transition

We have already reported that, in the vicinity of ρ_0, the strong interplay between clusters and uniform matter which are not allowed to occupy the same volume is responsible for a homogeneous-unhomogeneous matter transition. Its fingerprints have been already visible in Figs. 10, 11, and 14.

A more suited representation is given in the left panels of Figs. 15 and 16 where the relative baryonic density of uniform matter $\rho^{(HM)}/(w^{(HM)}\rho^{(HM)} + w^{(cl)}\rho^{(cl)})$ is expressed as a function of total baryonic density. The considered temperatures and proton fractions are T=1.6, 5 and 10 MeV and, respectively, Y_p=0.2 (Fig.15) and 0.3 (Fig.16). The common pattern of these curves is a sudden jump towards $\rho^{(HM)}/\rho = 1$ taking place at $\rho \lesssim \rho_0$ and a much smoother increase towards 1 at much smaller values of total density. This means that close to normal nuclear density and at low total densities, uniform nuclear matter dominates. While for the low density domain the SNA statement is true in the strict sense, in GCA it should be rather understood as the dominance of free nucleons over clusters. As we have already seen, in GCA clusters survive, by construction, in the whole density-temperature domain, but at low densities they represent a negligible percentage of matter.

With the exception of T=1.6 MeV where Monte-Carlo GCA convergence problems prevent accurate determination of the transition point, SNA and GCA predictions agree well. Both models show that the transition density depends on the temperature, but, at least in the presently investigated range, only slightly on Y_p.

The interesting point here is that this transition is spontaneously obtained in our model without performing an external artificial Maxwell construction at high density, as it is necessary in standard NSE models [42–44].

Refs. [80, 81] show that the homogeneous-unhomogeneous transition density, as well as the neutron skin thickness, depends upon the density dependence of the symmetry energy and, more precisely, upon $L = 3\rho_0 \left(\partial S_2\left(\rho\right) / \left(\partial\rho\right)\right)|_{\rho=\rho_0}$ where $S_2\left(\rho\right) = \left(\partial^2\left(E/A\right)/2\partial\beta^2\right)|_{\beta=0}$ with $\beta = (\rho_n - \rho_p)/\rho$. To check to what extend this cold matter result holds at finite temperature, we have calculated the transition region for T=5 MeV also in the case in which homogeneous matter is described by Sly230a [79] instead of SKM*. The result plotted with open diamonds in Figs. 15 and 16 shows
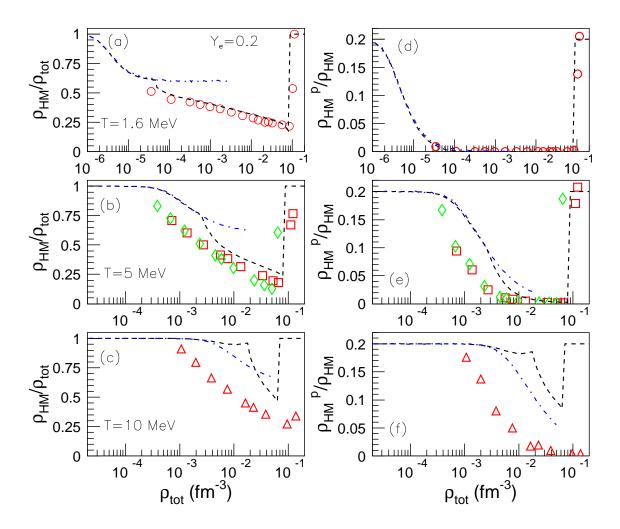
FIG. 15: (Color online) Evolution with total baryonic density of relative baryonic density in uniform matter (left panels) and free proton fraction (right panels) for T=1.6, 5 and 10 MeV and Y_e=0.2. Open circles, squares and triangles correspond to the predictions of the present model when uniform matter is calculated according to SKM*; dashed lines stand for Lattimer-Swesty data from Ref. [74]; dot-dashed lines correspond to Horowitz-Schwenk results based on the virial expansion of the equation of state [75]; open diamonds at T=5 MeV correspond to present model predictions in the case in which the uniform matter is calculated according to Sly230a [79].

no significative modification with respect to the previous ones. Given that L(SKM*)=46 MeV and L(Sly230a)=43.9 MeV, we partially confirm the conclusions of Refs. [80, 81]. In addition to this, within our model the transition density as well as the proton enrichment of the uniform matter could, at least in principle, depend also on how the clusterized matter component is implemented.

The isospin composition of uniform matter as a function of ρ is illustrated in the right panels of Figs. 15 and 16 for the same values of temperature and Y_p as above. Outside the transition region, where homogeneous matter dominates, $\rho_p^{(HM)}/\rho^{(HM)}$ approaches the total system proton fraction, Y_e. Inside the transition region, clusters proton enrichment (right panels of Fig. 10) makes uniform matter be depleted in protons. As the clusterized sub-system, free proton fractions keep the memory of total system proton fraction. In what regards the sensitivity on how homogeneous matter is implemented, the open diamonds show that SKM* and Sly230a give comparable results.

In what concerns the virial expansion of the equation of state as performed in Ref. [75], it is clear that the condition of sub-unitary nucleon and alpha fugacities prevents the exploration of ρ_{HM}/ρ_{tot} and ρ_{HM}^p/ρ_{HM} vs. ρ up to normal nuclear density. Nevertheless, over the accessible density domain the behavior of the two quantities clearly reproduces the already discussed patterns, that is (1) within a restrained density domain, which shrinks with increasing temperature, clusterized matter (alpha matter, in this case) dominates over homogeneous matter and (2) homogeneous matter is depleted in protons. As expected, the evolution with density of the two quantities is smooth
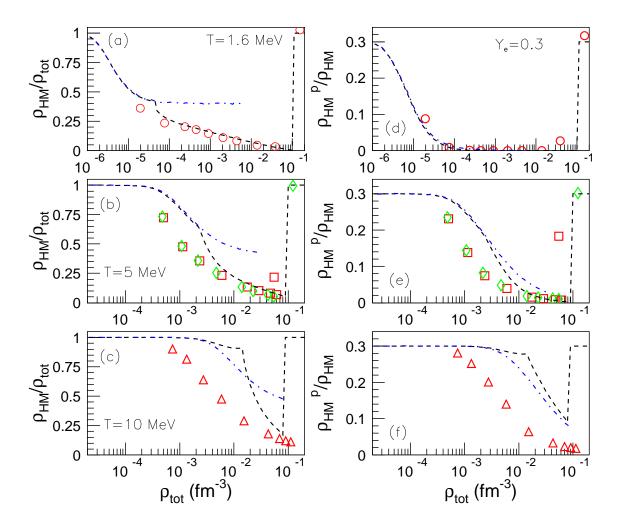
FIG. 16: (Color online) The same as in Fig. 15 for $Y_e = 0.3$.

and the lack of nuclei heavier than alpha leads to less mass bound in clusters with respect to both LS and the presently proposed model. The relative amount of alpha matter and its isospin symmetry make homogeneous matter have a proton fraction similar (T=1.6 MeV), higher (T=5 MeV) or in between (T=10 MeV) the values predicted by LS and the present model.

3. Equations of state

In astrophysical simulations, the equations of state, *i.e.* the functional dependences between different state observables, are extremely important ingredients.

Figs. 17 and 18 present the baryonic energy per baryon, $E^{(bar)}/A_b = \left(E^{(cl)} + E^{(HM)} \right)/A_b$, and, respectively, total energy per baryon, $E_{(tot)}/A_b = \left(E^{(bar)} + E^{(el)} + E^{(\gamma)} \right)/A_b$, as a function of total baryonic density for T=1.6, 5 and 10 MeV and Y_p=0.2 and 0.3.

As one may notice, at all considered temperatures the $E^{(bar)}/A_b(\rho)$ curves behave similarly: at low densities, they are flat as dominated by the ideal gas character of diluted homogeneous matter, while in the transition density, they manifest a sharp fall. LS results additionally show that for $\rho > \rho_0$ $E^{(bar)}/A_b$ rises steeply with ρ. The dependence with isospin asymmetry and temperature is trivial: more symmetric systems are more bound and average baryon energy increases with the temperature. Concerning the comparison between our model and LS, one can say that at T=1.6 MeV they agree perfectly. At higher temperatures the two models results deviate in the total baryonic density range corresponding to the homogeneous-unhomogeneous matter transition. Moreover, the discrepancy augments
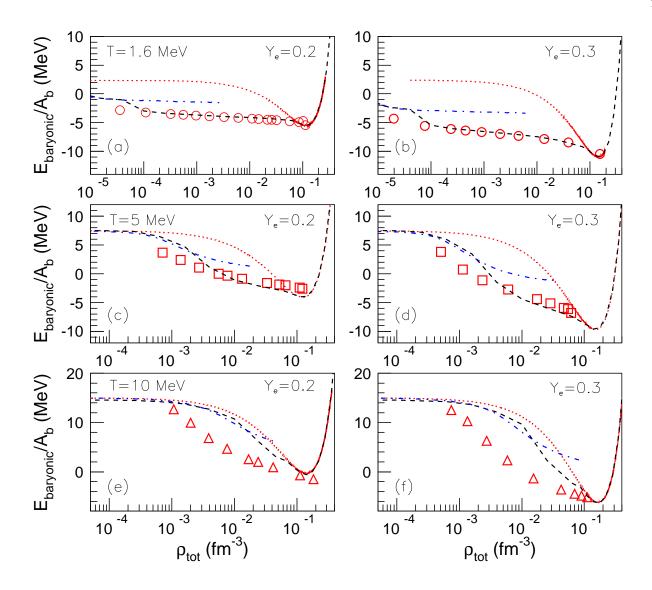
FIG. 17: Evolution with total baryonic density of the baryonic energy per baryon at different temperatures T=1.6, 5 and 10 MeV for Y_e=0.2 (left panels) and Y_e=0.3 (right panels). Open symbols correspond to present model predictions; dashed lines stand for Lattimer-Swesty data [74]; dot-dashed lines illustrate Horowitz-Schwenk results [75]; dotted lines correspond to the case in which only homogeneous nuclear matter would exist.

with the temperature. Taking into account that uniform matter is described by the same equation of state in LS and present model, the only possible explanation of the observed behavior concerns the clusterized component. As we have already discussed that the present model accounts for a systematically larger mass fraction bound in clusters with respect with LS, the clusters binding energy is expected to act in the sense of diminishing $E^{(cl)}$. This is confirmed by inspection of the thin lines in Fig. 17, which represent the baryonic energy per baryon number, obtained by artificially switching off the cluster component. For T=10 MeV, the thin line perfectly agrees with LS results, showing that in SNA clusters practically do not contribute to the EOS at high temperatures.

We have already seen (middle panels of Fig. 14) that in the high density sub-region of the transition density region HS accounts for a smaller fraction of mass bound in clusters with respect LS, while in the low density sub-region the opposite holds. This relation is replicated in the density dependence of the baryonic energy per baryon: in the high density sub-region $(E_b/A_b)|_{HS} > (E_b/A_b)|_{LS}$ while in the low density region $(E_b/A_b)|_{HS} \leq (E_b/A_b)|_{LS}$. Concerning the comparison of HS versus the present model, a similar conclusion may be drawn: as far as our model accounts for a higher percentage of bound mass, it predicts smaller values of E_b/A_b. In addition to this, HS shows less Y_e-sensitivity than the other two models.
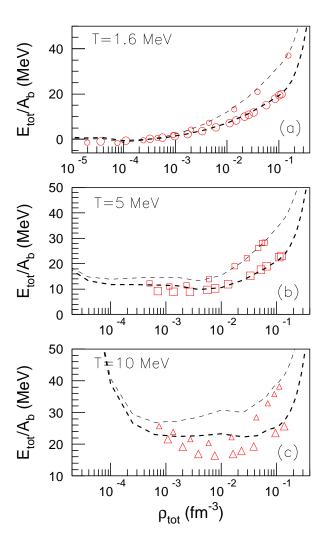
FIG. 18: Evolution with total baryonic density of the total energy per baryon at different temperatures T=1.6, 5 and 10 MeV and Y_e=0.2, 0.3. Open symbols illustrate present model predictions while dashed lines stand for Lattimer-Swesty data [74]. Large (small) symbols and thick (thin) lines correspond to Y_e=0.2 (0.3).

As the electron and photon contributions are trivial, it is obvious that all features of the baryonic energy density will be the same in the representation of the total energy per baryon. Indeed, Fig. 18 shows that at low temperatures and whatever densities, the present model results agree with the LS ones. The same is true for high temperatures and densities corresponding to homogeneous matter. Otherwise, GCA results deviate from the SNA ones.

Information on the density dependence of the baryonic energy for different system asymmetry allows one to infer the density dependence of the symmetry energy, an extremely important quantity which is so far largely unknown. Indeed, recasting the first term in the expansion of the internal energy per baryon in powers of asymmetry $\delta = (N - Z)/A$,

$$E_{sym}(\rho,T)/A = \frac{1}{2}\frac{\partial^2(E/A)}{\partial\delta^2}|_{\delta=0}, \tag{51}$$

in a finite difference formula, one gets,

$$E_{sym}(\rho,T)/A = \frac{E(\rho,T,Y_p^1)/A - E(\rho,T,Y_p^{(2)})/A}{(1 - 2Y_p^1)^2 - (1 - 2Y_p^2)^2}. \tag{52}$$

Eq. (52) is exact because of the quadratic dependence of the baryonic density with the isospin asymmetry. The model predictions on the baryonic density dependence of the symmetry energy per baryon (open symbols) are illus-
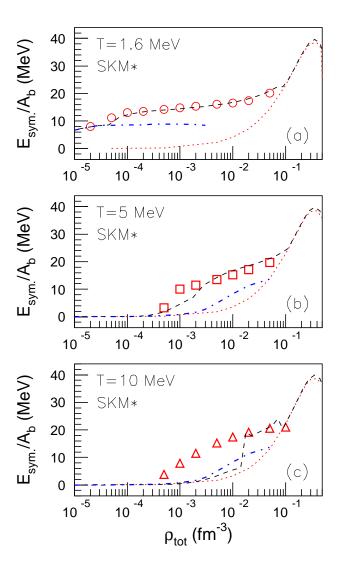
FIG. 19: Evolution with total baryonic density and temperature of the symmetry energy per baryon calculated according to Eq. (52). See Fig. 17 for the line and symbol code.

trated in Fig. 19 along with the Lattimer-Swesty (dashed lines), Horowitz-Schwenk (dot-dashed lines) and homogeneous matter (dotted lines) results. The common feature of the three models is that, when a significant amount of matter is bound in clusters, E_{sym}/A deviates from expectations based on homogeneous matter behavior. The deviation is visible in diluted matter and is washed out while approaching ρ_0, as nuclei and homogeneous matter are described by similar EOS. In addition to this remarkable symmetry energy increase, clusterization induces also a temperature dependence of $E_{sym}/A(\rho)$, not present in homogeneous matter. At the highest temperature, where our model accounts for much more clusters with respect to LS and HS, the agreement is mainly qualitative. At T=1.6 and 5 MeV the results of the present model perfectly agree with those of LS and both exceed the HS predictions. The same conclusions have been recently pointed out in Ref. [50]. There it is shown that clusterization also reduces the sensitivity of the EOS to the parameters of the effective interaction.

Figs. 20 and 21 illustrate the total baryonic density dependence of the baryonic entropy per baryon, $S^{(bar)}/A_b = (S^{(cl)} + S^{(HM)})/A_b$ and total entropy per baryon $S_{tot}/A_b = (S^{(bar)} + S^{(el)} + S^{(\gamma)})/A_b$ for T=1.6, 5 and 10 MeV and Y_e=0.2, 0.3. Both curve families present a monotonic decrease with ρ, a monotonic increase with T and an isospin asymmetry dependence which vanishes with increasing T. Again, at high temperatures and densities corresponding to the transition region, the predictions of our model are typically different than LS results, while the two calculations agree well outside the transition region and at low temperatures. The fact that at T=10 MeV the thin line, corre-
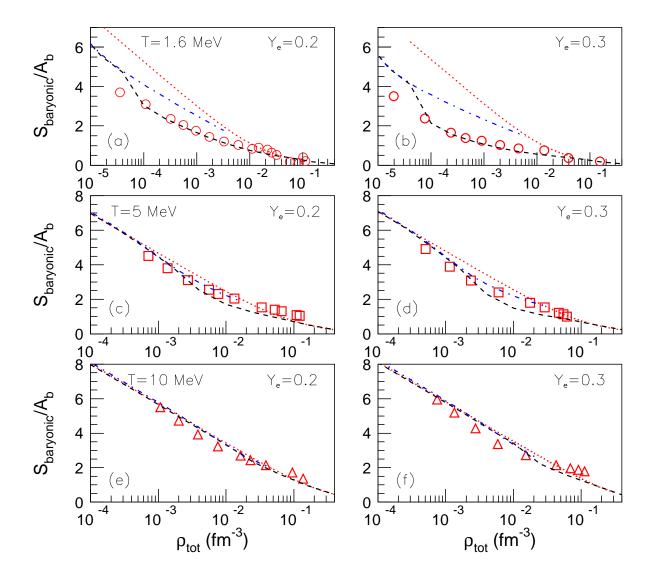
FIG. 20: The same as in Fig. 17 but for the baryonic entropy. See Fig. 17 for the line and symbol code.

sponding to the case in which baryonic matter would exclusively consist of uniform matter, sits perfectly on top of LS, reflects the different roles played by the clusterized component in the two models. The fact that at low temperatures HS results exceed the LS ones may be explained by the much increased cluster number within the first model (see the right panels of Fig. 14). This discrepancy diminishes with increasing temperature such at T=10 MeV, HS and LS results are practically identical. As in the case of energy, the total entropy inherits the characteristics of the baryonic term. Baryonic and total entropies show less sensitivity to clusters respect to the energy.

Figs. 22 and 23 present the dependence on the total baryonic density of the baryonic pressure $p^{(bar)} = w_{cl}p^{(cl)} + w_{HM}p^{(HM)}$ and, respectively, total pressure $p = p^{(bar)} + p^{(lattice)} + p^{(el)} + p^{(\gamma)}$ for the same temperatures and proton fractions considered before. For dilute matter $p^{(bar)}(\rho)$ is a linear function, as the system recovers the ideal gas limit. A spectacular feature of the LS results is that, up to a certain temperature, at a certain value of ρ which depends on the temperature $p^{(bar)}(\rho)$ manifests a sudden fall.

This behavior is due to those solutions of the uniform matter component which are unstable and, thus, characterized by negative values of $p^{(HM)}$. If baryonic matter would be exclusively made out of homogeneous matter, $p^{(bar)}(\rho_{tot})|_{Y_e}$ would correspond to the dotted lines in Fig. 22. Their shape is qualitatively similar to LS but, except for T=10 MeV, quantitative discrepancies exist over the whole density range, as one would have actually expected given the cluster contribution.

Quite interesting, the falling pattern of HM and LS pressure curves practically does not exist within our model. The
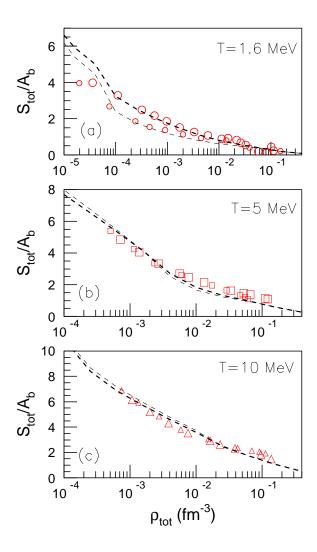
FIG. 21: The same as in Fig. 18 but for the total entropy. See Fig. 18 for the line and symbol code.

explanation relies on the mixture stability criterion we have adopted in order to maximize the (constrained) entropy (see Section IIA1). A reminiscence of the fall may, nevertheless, be noticed in the short plateaus or back-bendings. HS results plotted with dot-dashed lines in the left panels do not manifest signatures of negative pressure, either, meaning that the nuclear matter obtained by performing a virial expansion of the equation of state is stable.

The disappearance of the sudden fall at high temperatures (in our case $T=10$ MeV) may be understood looking again at Fig. 3. This figure shows that if the $\mu_n - \mu_p$ trajectory through the phase diagram fixed by the clusterized system is systematically situated under the high density spinodal limit, then only one solution for the uniform nuclear matter will exist, namely the low density stable solution.

Fig. 23 correspond to p_{tot} vs. ρ, and show that after considering the electron and photon contributions the discrepancies originating from the baryonic component of the EOS are to a large extent washed out. The same conclusion was reached by Refs. [42, 51].

C. Neutrino opacity

Abundant neutrino fluxes are emitted during the collapse of a supernova core and in the first 10^5 years of life of the subsequently born neutron star, being thus the main responsible for the star cooling. The mean free path of the neutrinos depends on the EOS and baryonic composition. During the collapse phase, it decreases as the star radius shrinks from 100 km to 10 km, such that it eventually becomes smaller than the star radius. This final regime
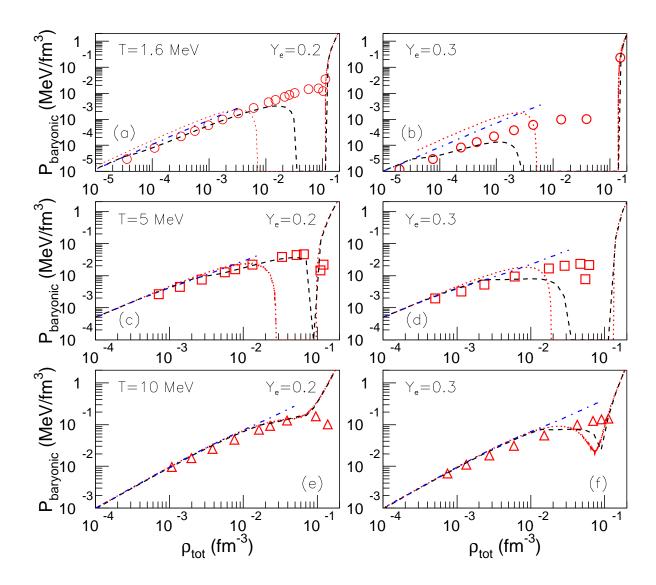
FIG. 22: The same as in Fig. 17 but for the baryonic pressure, $p_b = w_{cl}p^{(cl)} + w_{HM}p^{(HM)}$. See Fig. 17 for the line and symbol code.

corresponds to the so-called full neutrino trapping, while the initial stage corresponds to neutrino transparency and is characterized by a vanishing neutrino chemical potential. Full neutrino trapping is expected to occur also in post-bounce supernovae, when the matter is still dense. The transition between neutrino trapping and neutrino free streaming should in principle be a continuous process, obtained by solving the Boltzmann equation for neutrino transport coupled with the hydrodynamics of the supernova evolution[82]. In many actual simulations, schematic flux-limiting schemes are adopted in the diffusion approximation[83] allowing regimes of partial neutrino trapping. In these modelizations the neutrino diffusion coefficient depends on the neutrino mean free path, which in turn obviously depends on the matter composition through the different elastic and inelastic scattering processes of neutrinos on protons and nuclei[32, 82].

In Ref. [71] it was additionally suggested that the matter composition itself may depend in turn on the percentage of trapped neutrinos, thus introducing a self-consistency problem.

To explore this issue, we study in this section the composition of the baryonic matter in our model as a function of the trapped neutrino density.

The total number of neutrinos produced per unit volume ρ_ν^{prod} can be calculated from the (local) proton fraction considering hot star matter as produced from the deleptonization of an initial iron core according to [71]
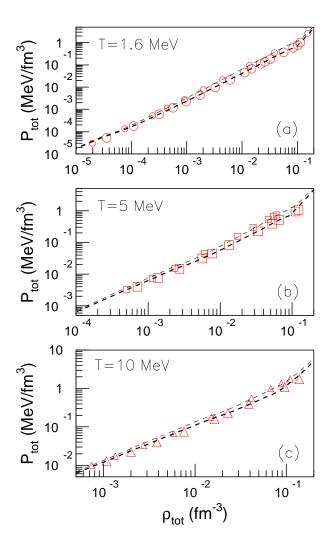
FIG. 23: The same as in Fig. 18 but for the total pressure, $p_{tot} = w_{cl}p^{(cl)} + w_{HM}p^{(HM)} + p^{(lattice)} + p^{(el)} + p^{(\gamma)}$. It is remarkable to notice that by summing up the electron and gamma contribution, the total EOS shows almost no sensitivity to the baryonic EOS. See Fig. 18 for the line and symbol code.

$$\rho_\nu^{prod} = \rho \left[\left(\frac{Z}{A} \right)_0 - \left(\frac{Z}{A} \right) \right], \tag{53}$$

where $(Z/A)_0$ stands for the Z/A in ^{56}Fe.

The percentage of trapped neutrinos x_ν depends on time and on the local neutrino mean free path. Determining this quantity consistently would require a full hydrodynamic calculation with a complete treatment of the weak processes implied, which is completely out of scope of the present paper. To study the interplay between trapping and matter composition we simply take the neutrino density ρ_ν at the given thermodynamic condition as a free parameter, linked to the opacity x_ν by $x_\nu \equiv \rho_\nu/\rho_\nu^{prod}$. The scope of this analysis will then be to check whether the matter composition depends on the neutrino density, which would imply an extra self-consistent coupling between the baryon and the lepton sector. Indeed if the cluster properties strongly vary during the transition between neutrino trapping and neutrino streaming, it would be necessary to couple the neutrino propagation with the calculation of the EOS, which would be a very heavy numerical task.

Eq. (40) in Section IID shows that for a relativistic Fermi gas the particle density is univocally linked to its chemical potential. In the case of neutrinos, one can safely use the simpler $T=0$ expression of an ultra-relativistic degenerate
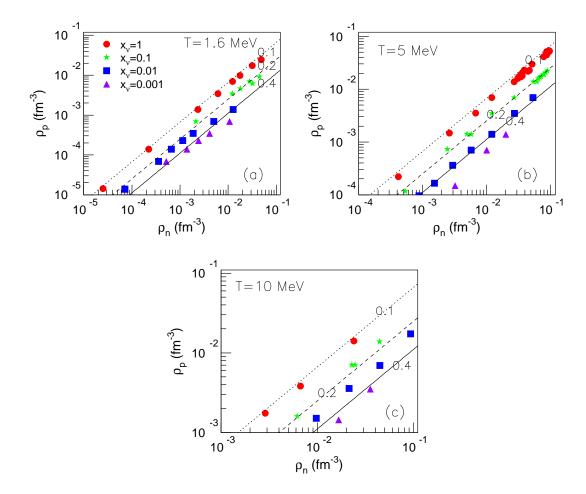
FIG. 24: (Color online) Constant neutrino opacity ($x_\nu = 1, 10^{-1}, 10^{-2}, 10^{-3}$) paths in the total density plane for T=1.6, 5 and 10 MeV under the assumption of β-equilibrium. Neutrino opacity is calculated according to Eq. (53). The lines correspond to paths of constant Z/A, whose values are indicated on the figure.

Fermi gas:

$$\mu_\nu = \hbar c \left(6\pi^2 \rho_\nu\right)^{1/3} . \tag{54}$$

The beta equilibrium equation (44) with a neutrino chemical potential $\mu_\nu(\rho_\nu)$ fixed from eq.(54) such as to produce the chosen neutrino density $\rho_\nu = x_\nu \rho_\nu^{prod}$, defines a trajectory in the (μ_n, μ_p), or equivalently (ρ_n, ρ_p) plane.

These trajectories are shown in Fig. 24 for different values of x_ν , covering the whole domain between full trapping $x_\nu = 1$ and zero trapping $x_\nu = 0$.

As one may remark, the constant x_ν paths roughly correspond to constant Z/A paths (lines on the figure). Moreover, the global isospin asymmetry of the matter increases monotonically with the percentage of trapped neutrinos and no significant dependence on temperature is observed. For instance, over the whole considered temperature domain the full neutrino trapping path lies along the $Z/A = 0.1$ path, while $x_\nu = 10^{-3}$ corresponds to Z/A slightly higher than 0.4. These results are in good agreement with Ref. [71], where only homogeneous nuclear matter was considered and no clusters were included.

The extra information beared by the present work is that we can correlate the percentage of trapped neutrinos with the characteristics of the clusters.

Fig. 25 displays the average cluster size (left panels) and isospin composition (right panels) as a function of total baryonic density at different temperatures along constant neutrino opacity paths. For the sake of completeness, no selection is now made with respect to the stability of the mixture. We can see that the size strongly depends on the thermodynamic conditions (temperature and density) but, in the cases in which homogeneous matter is stable, it
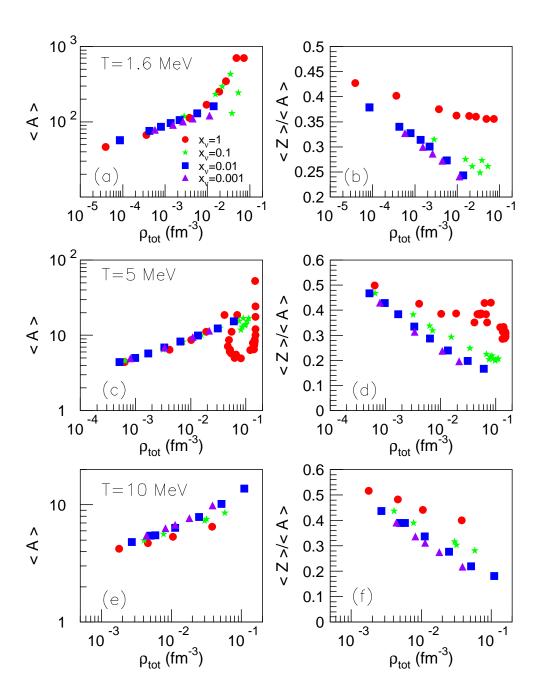
FIG. 25: (Color online) Average cluster size (left panels) and average cluster isospin (right panels) as a function of total baryonic density for T=1.6, 5 and 10 MeV along constant neutrino opacity ($x_\nu = 1, 10^{-1}, 10^{-2}, 10^{-3}$) paths under the assumption of β-equilibrium. No selection is performed with respect to the mixture stability.

is virtually independent of the opacity to neutrinos. This result can be understood from the fact that changing the percentage of trapped neutrinos at beta-equilibrium essentially amounts to changing the matter isospin asymmetry Y_p for a given total density ρ (see Fig. 24). In turn, this affects the chemical composition of clusters but not the cluster size, as we have already observed in discussing Fig. 10. Since the interaction probability of neutrinos with matter essentially depends on isoscalar quantities as the average cluster density and size [29, 32], our result indicates that the problem of neutrino-baryon interaction can be effectively decoupled from the problem of the matter composition.

IV. CONCLUSIONS

In this paper we have presented a phenomenological model for stellar matter at finite temperature and sub-saturation densities which describes matter inhomogeneities as a continuous mixture of a distribution of loosely interacting clusters in statistical equilibrium, with free nucleons treated within the non-relativistic mean-field approximation. The two components interact through the electrostatic energy in the Wigner-Seitz approximation, and a configuration-dependent excluded volume term in the spirit of the Van-der-Waals gas.

Such mixture is demonstrated to minimize (maximize) the associated energetic (entropic) thermodynamic potential in the whole considered range of densities and temperature such that a stable solution can always be found. As a consequence, the transition from the homogeneous core to the inhomogeneous crust of a finite temperature neutron star is naturally obtained in the model, at variance with other approaches where discontinuous transitions have to be invoked.

In qualitative agreement with previous works based on nuclear statistical equilibrium (NSE), we find that the inclusion of a statistical distribution of clusters in low-density stellar matter modifies in an important way the average matter composition respect to standard treatments as the LS equation of state. For densities close to the transition density which are not accessible to NSE models in a thermodynamically consistent way, we show that clustering has also sizeable consequences of thermodynamic quantities and equations of state. In particular both the symmetry energy and the baryonic energy are considerably altered by the presence of clusters, in agreement with the microscopic results of Ref. [50].

These results open different perspectives for future work which will be pursued in the next future.

Our formalism where the cluster partition sum is sampled within an exact, though numerical, Monte-Carlo procedure, allows to account for cluster correlations. We have already shown in a previous paper [63] that going beyond the non-interacting NSE approximation for cluster equilibrium has an important effect on the cluster phase diagram, and in the present work the configuration-dependent excluded volume correction, which phenomenologically accounts for the nuclear interaction, was shown to be responsible of the crust-core transition. The Coulomb part of the interaction, which is presently treated in the usual one-body Wigner-Seitz approximation, could also be calculated exactly accounting for charge fluctuations inside the Wigner-Seitz cell. From the existing literature [16, 84] we expect that properly accounting for Coulomb correlations induced by the charge fluctuations at the microscopic level may have an important influence on matter composition and thermodynamic features, particularly at high density and temperature where the configuration fluctuations are maximal.

In the regime of baryonic density close to saturation, we observe metastable and unstable solutions corresponding to bubble-like structures where small spherical clusters coexist with slightly diluted homogeneous matter. The possible persistence at high temperature of pasta-like structures, well documented at low temperature [12–14], is still an open question and it will be interesting to see if such exotic structures appear if deformation degrees of freedom are allowed in the configuration geometry and cluster energy functional.

Concerning the cluster energy functional, in this exploratory work we have employed a very simple and simplistic liquid-drop based expression. It will however be very easy to implement a composite functional giving the experimental masses at zero temperature and vanishing density, and evolving towards a parametric formulation at high density and temperature and for unknown neutron-rich nuclear species.

Concerning the homogeneous matter functional, we plan to include pairing correlations within the finite temperature HFB approach as a natural extension of the present formalism, which will allow having a trustable equation of state at the lowest temperatures.

Finally, once the different physical inputs will be well settled, a longer range project consists in constructing a complete EOS table for direct implementation in supernova and neutron stars codes, in the framework of the COMPSTAR project [85].

ACKNOWLEDGEMENTS

[1] R. Knorren, M. Prakash and P.J. Ellis, Phys. Rev. **C52**, 3470 (1995).
[2] T. Takatsuka, S. Nishizaki, Y. Yamamoto and R. Tamagaki, Prog.Theor.Phys. **115**, 355 (2006).
[3] D. Page, M. Prakash, J. M. Lattimer, and A. W. Steiner, Phys. Rev. Lett. **85**, 2048 (2000).
[4] D. Blaschke, T. Klähn, and D. N. Voskresensky, Astrophys. J. **533**, 406 (2000).
[5] P. K. Panda, D. P. Menezes, and C. Providencia, Phys. Rev. **C69**, 058801 (2004).
[6] O. E. Nicotra, M. Baldo, G. F. Burgio, and H. J. Schulze, Phys. Rev. **D74**, 123001 (2006).
[7] K. Nakazato, K. Sumiyoshi, and S. Yamada, Phys. Rev. **D77**, 103006 (2008).
[8] N. Yasutake, T. Maruyama and T. Tatsumi, Phys. Rev. **D80**, 123009 (2009).
[9] J. M. Lattimer and M. Prakash, Science Vol. **304** no. 5670, 536 (2004).
[10] P.Haensel,A.Y.Potekhin,D.G.Yakovlev, *'Neutron stars: equation of state and structure'*, Springer, Berlin (2007).
[11] C.J. Horowitz, M.A. Pérez-Garcia, D.K. Berry and J. Piekarewicz, Phys. Rev. **C 72**, 035801 (2006).
[12] H. Sonoda, G. Watanabe, K. Sato, K. Yasuoka and T. Ebisuzaki, Phys. Rev. **C 77**, 035806 (2008); G. Watanabe, H. Sonoda, T. Maruyama, K. Sato, K. Yasuoka and T. Ebisuzaki, Phys. Rev. Lett. **103**, 121101 (2009).
[13] W. G. Newton and J. R. Stone, Phys. Rev. **C 79**, 055801 (2009).
[14] F. Sebille, S. Figerou and V. de la Mota, Nucl. Phys. **A 822**, 51 (2009).
[15] M. Grousson, G. Tarjus and P. Viot, Phys. Rev. **E 62**, 7781 (2000); M. Grousson, G. Tarjus and P. Viot, Phys. Rev. **E 64**, 036109 (2001).
[16] P. Napolitani, Ph.Chomaz, F. Gulminelli and K.Hasnaoui, Phys. Rev. Lett **98**, 131102 (2007); C. Ducoin, K. Hasnaoui, P. Napolitani, Ph.Chomaz and F. Gulminelli, Phys. Rev. **C 75** 065805 (2007).
[17] J. M. Lattimer, C. J. Pethick, D. G. Ravenhall and D. Q. Lamb, Nucl. Phys. **A432**, 646 (1985).
[18] M. Lassaut, H. Flocard, P. Bonche, P. H. Heenen, and E. Suraud, Astron. Astrophys. **183**, L3 (1987).
[19] C. J. Pethick, D. G. Ravenhall, C. R. Lorenz, Nucl. Phys. **A 584**,675 (1995).
[20] F. Douchin and P. Haensel, Phys. Lett. **B485**, 107 (2000).
[21] G. Watanabe, K. Iida, and K. Sato, Nucl. Phys. **A726**, 357 (2003).
[22] T. Maruyama, T. Tatsumi, D. N. Voskresensky, T. Tanigawa, and S. Chiba, Phys. Rev. **C 72**, 015802 (2005).
[23] J. M. Lattimer and F. Douglas Swesty, Nucl. Phys. **A535**, 331 (1991).
[24] H. Shen, H. Toki, K. Oyamatsu and K. Sumiyoshi, Nucl. Phys. **A 637**, 435 (1998); H. Shen, H. Toki, K. Oyamatsu and K. Sumiyoshi, Prog. Theor. Phys. **100**, 1013 (1998).
[25] G. Shen, C. J. Horowitz and S. Teige, Phys. Rev. **C 82**, 015806 (2010).
[26] A. Burrows and J. M. Lattimer, Astrophys. Journ. **307** (1986) 178.
[27] H. A. Bethe, G. E. Brown, J. Applegate and J. M. Lattimer, Nucl. Phys. **A324**, 487 (1979).
[28] Ya. B. Zeldovich and I. D. Novikov, *'Relativistic Astrophysics'*, University of Chicago press, Chicago (1971).
[29] C. J. Horowitz, M. A. Pérez-Garcia, J. Carriere, D. K. Berry and J. Piekarewicz, Phys. Rev. **C 70**, 065806 (2004).
[30] G. Martínez-Pinedo, M. Liebendorfer and D. Frekers, Nucl. Phys. **A777**, 395 (2006).
[31] H. T. Janka, K. Langanke, A. Marek, G. Martínez-Pinedo, and B. Müller, Phys. Rep. **442**, 38 (2007).
[32] H. Sonoda, G. Watanabe, K.Sato, T. Takiwaki, K. Yasuoka, T. Ebisuzaki. Phys. Rev. **C 75**, 042801(R) (2007).
[33] W. R. Hix, O. E. B. Messer, A. Mezzacappa, M. Liebendorfer, J. Sampaio, K. Langanke, D. J. Dean, and G. Martínez-Pinedo, Phys. Rev. Lett. **91**, 201102 (2003).
[34] K. Langanke and G. Martínez-Pinedo, Nucl. Phys. **A731**, 365 (2004).
[35] J. J. Cowan, F. K. Thieleman and J. W. Truran, Phys. Rep. **208**, 267 (1991).
[36] Y. Z. Qian, Prog. Part. Nucl. Phys. **50**, 153 (2003).
[37] J.Margueron, J.Navarro and P.Blottiau, Phys. Rev. **C 70**, 028801 (2004).
[38] O. L. Caballero, C. J. Horowitz and D. K. Berry, Phys. Rev. **C 74**, 065801 (2006).
[39] D. Page, U. Geppert and F. Weber Nucl. Phys. **A 777**, 497 (2006).
[40] D. G. Yakovlev, O. Y. Gnedin, M. E. Gusakov, A. D. Kaminker, K. P. Levenfish and A. Y. Potekhin, Nucl. Phys. **A 752**, 590 (2005).
[41] A.C.Phillips, *The Physics of Stars*, John Wiley and Sons, Chichester, GB (1994).
[42] A. S. Botvina, I. N. Mishustin, Nucl. Phys. **A 843**, 98 (2010).
[43] S. I. Blinnikov, I. V. Panov, M. A. Rudzsky and K. Sumiyoshi, arXiv: 0904.3849 [astro-ph].
[44] S. R. Souza, A. W. Steiner, W. G. Lynch, R. Donangelo and M. A. Famiano, Astrophys. J. **707**, 1495 (2009).
[45] M. E. Fisher, Physics (NY) **3**, 255 (1967).
[46] J. Negele and D. Vautherin, Nucl. Phys. **A 207**, 298 (1973).
[47] S. K. Samaddar, J. N. De, X. Vinas and M. Centelles, Phys. Rev. **C 80**, 035803 (2009).
[48] A. Arcones, G. Martínez-Pinedo, E. O'Connor, A. Schwenk, H. Th. Janka, C. J. Horowitz, K. Langanke, Phys. Rev. **C 78**, 015806 (2008).
[49] S. Heckel, P. P. Schneider and A. Sedrakian, Phys. Rev. **C 80**, 015805 (2009).
[50] S. Typel, G. Röpke, T. Klÿähn, D. Blaschke and H. H. Wolter, Phys. Rev. **C 81**, 015803 (2010).
[51] M. Hempel and J. Schaffner-Bielich, Nucl. Phys. **A 837**, 210 (2010).
[52] D. Vautherin, Adv. Nucl. Phys. **22**, 123 (1996).
[53] C. Ducoin, Ph. Chomaz and F. Gulminelli, Nucl. Phys. **A 771**, 68 (2006).
[54] M. Barranco and J. R. Buchler, Phys. Rev. **C 24**, 1191 (1981).

[55] S. Shlomo and V. M. Kolomietz, Rep. Prog. Phys. **68**, 1 (2005).

[56] F. Douchin, P. Haensel and J. Meyer, Nucl. Phys. **A 665**, 419 (2000).

[57] A. Rios, Nucl. Phys. **A 845**, 58 (2010).

[58] J. Bartel, P. Quentin, M. Brack, C. Guet and H. B. Hakansson, Nucl. Phys. **A386**, 79 (1982).

[59] J. P. Bondorf, A. S. Botvina, A. S. Iljinov, I. N. Mishustin and K. Sneppen, Phys. Rep. **257**, 133 (1995).

[60] D. H. E. Gross, Rep. Progr. Phys. **53**, 605 (1990).

[61] S. E. Koonin and J. Randrup, Nucl. Phys. A **474**, 173 (1987).

[62] Al. H. Raduta and Ad. R. Raduta, Phys. Rev. C **55**, 1344 (1997); *ibid.* Phys. Rev. C 65, 054610 (2002).

[63] Ad. R. Raduta and F. Gulminelli, Phys. Rev. C **80**, 024606 (2009).

[64] G. Audi and A. H. Wapstra, Nucl. Phys. **A595**, 409 (1995).

[65] A. S. Iljinov, M. V. Mebel, N. Bianchi, E. de Sanctis, C. Guaraldo, V. Lucherini, V. Muccifora, E. Polli, A. R. Reolon and P. Rossi, Nucl. Phys. **A543**, 517 (1992).

[66] C. Ishizuka, A. Ohnishi, and K. Sumiyoshi, Prog. Theor. Phys. Suppl. **146**, 373 (2002).

[67] N. K. Glendenning, Phys. Rep. **342**, 394 (2001).

[68] M. Hempel, G. Pagliara, J. Schaffner-Bielich, Phys. Rev. **D 80**, 125014 (2009).

[69] D.H.E. Gross, *'Microcanonical Thermodynamics: Phase Transitions in Finite Systems'*, Lecture Notes in Physics, vol. **66**, World Scientific (2001).

[70] J. Margueron and A. Fantina, private communication.

[71] C. Ducoin, Ph. Chomaz and F. Gulminelli, Nucl. Phys. **A789**, 403 (2007).

[72] F. S. Kitaura, H. Th. Janka and W. Hillebrandt, Astron. Astrophys. **450**, 345 (2006).

[73] A. Marek and H. Th. Janka, Astrophys. Journ. **694**, 664 (2009).

[74] J. M. Lattimer, http://www.astro.sunysb.edu/lattimer/EOS/key.txt

[75] C. J. Horowitz and A. Schwenk, Nucl. Phys. **A776**, 55 (2006).

[76] M. D'Agostino, F. Gulminelli, Ph. Chomaz, M. Bruno, F. Cannata, A. Bonasera, R. Bougault, F. Gramegna, I. Iori, N. Le Neindre, G. V. Margagliotti, P. F. Mastinu, P. M. Milazzo, A. Moroni, G. Vannini, Phys. Lett. **B 473**, 219 (2000).

[77] F. Gulminelli and M. D'Agostino, Eur. Phys. Journ. **A 30**, 253 (2006).

[78] E. Bonnet, D. Mercier, B. Borderie, F. Gulminelli, M. F. Rivet and B. Tamain, Phys. Rev. Lett. **103**, 072701 (2009).

[79] E. Chabanat, P. Bonche, P. Haensel, J. Meyer and R. Schaeffer, Nucl. Phys. **A627**, 710 (1997).

[80] C. J. Horowitz and J. Piekarewicz, Phys. Rev. Lett. **86**, 5647 (2001).

[81] I. Vidana, C. Providencia, A. Polls and A. Rios, Phys. Rev. C **80**, 045806 (2009).

[82] M. Liebendorfer, M. Rampp, H. Th. Janka and A. Mezzacappa, Astrophys. J. **620**, 840 (2005).

[83] R. B. Bowers and J. R. Wilson, Astrophys. J. **263**, 366 (1982).

[84] G. Watanabe and K. Iida, Phys. Rev. **C 68**, 045801 (2003).

[85] COMPSTAR, european program 06-RNP-106 of the European Science Foundation, EOS construction task coordinated by M. Baldo, Y. Illarionov and M. Oertel.